Metal Complexes of Dithiolate Ligands: 5,6-Dihydro-1,4-dithiin-2,3-dithiolato ($dddt^{2-}$), 5,7-Dihydro-1,4,6-trithiin-2,3-dithiolato ($dtdt^{2-}$), and 2-Thioxo-1,3-dithiole-4,5-dithiolato ($dmit^{2-}$). Synthesis, Electrochemical Studies, Crystal and Electronic Structures, and Conducting Properties

Christophe Faulmann,[1a] Ahmed Errami,[1a] Bruno Donnadieu,[1a] Isabelle Malfant,[1a] Jean-Pierre Legros,[1a] Patrick Cassoux,*[,1a] Carme Rovira,[1b] and Enric Canadell[1c]

Equipe Précurseurs Moléculaires et Matériaux, Laboratoire de Chimie de Coordination du CNRS lié par convention à l'Université Paul Sabatier, 205 Route de Narbonne, 31077 Toulouse Cedex, France, Departament de Quimica Fisica, Facultat de Quimica, Universitat de Barcelona, 08028 Barcelona, Spain, Institut de Ciencia de Materials de Barcelona, Campus de la UAB, 08193 Bellaterra, Spain, and Laboratoire de Chimie Théorique (CNRS URA 506), Université de Paris-Sud, 91405 Orsay Cedex, France

Received January 11, 1996[⊗]

New precursors to potentially conductive noninteger oxidation state (NIOS) compounds based on metal complexes $[ML_2]^{n-}$ [M = Ni, Pd, Pt; L = 5,6-dihydro-1,4-dithiin-2,3-dithiolato ($dddt^{2-}$), 5,7-dihydro-1,4,6-trithiin-2,3-dithiolato ($dtdt^{2-}$), and 2-thioxo-1,3-dithiole-4,5-dithiolato ($dmit^{2-}$); $n = 2, 1, 0$] have been investigated. Complexes of the series $(NR_4)[ML_2]$ (R = Me, Et, Bu; L = $dddt^{2-}$, $dtdt^{2-}$) have been isolated and characterized, and the crystal structure of $(NBu_4)[Pt(dtdt)_2]$ (**1**) has been determined {**1** = $C_{24}H_{44}NPtS_{10}$, $a = 12.064(2)$ Å, $b = 17.201(3)$ Å, $c = 16.878(2)$ Å, $\beta = 102.22(2)°$, $V = 3423(1)$ Å^3, monoclinic, $P2_1/n$, $Z = 4$}. Oxidation of these complexes affords the corresponding neutral species $[ML_2]^0$. Another series of general formula $(cation)_n[M(dmit)_2]$ [cation = PPN^+, BTP^+, and $(SMe_yEt_{3-y})^+$ with $y = 0$, 1, 2, and 3, $n = 2$, 1, M = Ni, Pd] has also been studied. All of these $(cation)_n[M(dmit)_2]$ complexes have been isolated and characterized [with the exception of (cation)[Pd(dmit)$_2$] for cation = $(SMe_yEt_{3-y})^+$]. The crystal structures of $(PPN)[Ni(dmit)_2]\cdot(CH_3)_2CO$ (**2**) and $(SMeEt_2)[Ni(dmit)_2]$ (**3**) have been determined {**2** = $C_{45}H_{36}NNiS_{10}P_2O$, $a = 12.310(2)$ Å, $b = 13.328(3)$ Å, $c = 15.850(3)$ Å, $\alpha = 108.19(3)°$, $\beta = 96.64(2)°$, $\gamma = 99.67(2)°$, $V = 2373(1)$ Å^3, triclinic, $P\bar{1}$, $Z = 2$; **3** = $C_{11}H_{13}NiS_{11}$, $a = 7.171(9)$ Å, $b = 17.802(3)$ Å, $c = 16.251(3)$ Å, $\beta = 94.39(4)°$, $V = 2068(2)$ Å^3, monoclinic, $P2_1/n$, $Z = 4$} NIOS salts derived from the preceding precursors were obtained by electrochemical oxidation. Electrochemical studies of the $[M(dddt)_2]$ complexes show that they may be used for the preparation of NIOS radical cation salts and $[M(dddt)_2][M'(dmit)_2]_x$ compounds, but not for the preparation of $(cation)[M(dddt)_2]_z$ NIOS radical anion salts. The electrochemical oxidation of the $[M(dtdt)_2]^-$ complexes always yields the neutral $[M(dtdt)_2]^0$ species. The crystal structure of $[Pt(dddt)_2][Ni(dmit)_2]_2$ (**4**) has been determined and is consistent with the low compaction powder conductivity (5×10^{-5} S cm^{-1} at room temperature) {**4** = $C_{20}H_8Ni_2PtS_{28}$, $a = 20.336(4)$ Å, $b = 7.189(2)$ Å, $c = 14.181(2)$ Å, $\beta = 97.16(2)°$, $V = 2057(1)$ Å^3, monoclinic, $C2/m$, $Z = 2$}. The crystal structures of the semiconducting NIOS compounds $(BTP)[Ni(dmit)_2]_3$ (**5**) and $(SMe_3)[Ni(dmit)_2]_2$ (**6**) have been determined {**5** = $C_{43}H_{22}PNi_3S_{30}$, $a = 11.927(2)$ Å, $b = 24.919(2)$ Å, $c = 11.829(3)$ Å, $\alpha = 93.11(1)°$, $\beta = 110.22(1)°$, $\gamma = 83.94(1)°$, $V = 3284(1)$ Å^3, triclinic, $P\bar{1}$, $Z = 2$; **6** = $C_{15}H_9Ni_2S_{21}$, $a = 7.882(1)$ Å, $b = 11.603(2)$ Å, $c = 17.731(2)$ Å, $\alpha = 77.44(1)°$, $\beta = 94.39(1)°$, $\gamma = 81.27(1)°$, $V = 1563(1)$ Å^3, triclinic, $P\bar{1}$, $Z = 2$}. The parent compound $(SEt_3)[Ni(dmit)_2]_z$ (unknown stoichiometry) is also a semiconductor with a single-crystal conductivity at room temperature of 10 S cm^{-1}. By contrast, the single-crystal conductivity at room temperature of $(SMeEt_2)[Pd(dmit)_2]_2$ (**7**) is rather high (100 S cm^{-1}). **7** behaves as a pseudometal down to 150 K and undergoes an irreversible metal−insulator transition below this temperature. The crystal structure of **7** has been determined {**7** = $C_{17}H_{13}NPd_2S_{21}$, $a = 7.804(4)$ Å, $b = 36.171(18)$ Å, $c = 6.284(2)$ Å, $\alpha = 91.68(4)°$, $\beta = 112.08(4)°$, $\gamma = 88.79(5)°$, $V = 1643(1)$ Å^3, triclinic, $P\bar{1}$, $Z = 2$}. The electronic structure of $(SMeEt_2)[Pd(dmit)_2]_2$ (**7**) and the possible origin of the metal−insulator transition at 150 K are discussed on the basis of tight-binding band structure calculations.

Introduction

Most molecule-based superconductors, except the doped fullerenes A_xC_{60} (A = alkali and alkaline earth metals),[2] are charge transfer salts of only six organic molecules derived from tetrathiafulvalene (TTF), namely, MDT-TTF, TMTSF, BEDT-TTF, BEDO-TTF, BEDT-TSF, and DMET.[3,4] The largest family of organic molecule-based superconductors comprises

⊗ Abstract published in *Advance ACS Abstracts,* May 15, 1996.

(1) (a) Equipe Précurseurs Moléculaires et Matériaux. (b) Departament de Quimica Fisica. (c) Institut de Ciencia de Materials de Barcelona and Laboratoire de Chimie Théorique.

(2) (a) Hebard, A. F.; Rosseinsky, M. J.; Haddon, R. C.; Murphy, D. W.; Glarum, S. H.; Palstra, T. T. M.; Ramirez, A. P.; Kortan, A. R. *Nature* **1991**, *350*, 600. (b) Hebard, A. F. *Phys. B* **1994**, 197,544.

(3) Williams, J. M.; Ferraro, F. R., Thorn, R. J.; Carlson, K. D.; Geiser, U.; Wang, H. H.; Kini, A. M.; Whangbo, M.-H. *Organic Superconductors (Including Fullerenes)*; Prentice Hall: Englewood Cliffs, NJ, 1992.

(4) Cassoux, P.; Miller, J. S. in *Chemistry of Advanced Materials: A New Discipline*; Interrante, L. V., Hampden-Smith, M., Eds.; VCH Publishers: New York, in press.

S0020-1669(96)00034-1 CCC: $12.00

the $(BEDT\text{-}TTF)_2X$ salts [BEDT-TTF = bis(ethylenedithio)-tetrathiafulvalene; X = anions such as I_3^-, $[Cu(NCS)_2]^-$, and $\{Cu[N(CN)_2]Cl\}^-$].[3]

Yet, inorganic compounds, namely, the partially oxidized platinum complexes $K_2[Pt(CN)_4]X_{0.3}\cdot 3H_2O$ (X = Cl, Br),[5] were among the first molecule-based metal-like conductors. Other inorganic molecule-based systems have also been used for the fabrication of materials exhibiting high conductivities, including linear-chain iridium complexes,[6] macrocyclic metal complexes such as those derived from glyoximate and tetraazaannulene ligands,[7−9] metalloporphyrins,[7,10] DCNQI metal complexes,[11,12] and metal complexes of dithiolate ligands.[13,14] However, superconductivity has been observed in only seven charge transfer salts of metal complexes of just one 1,2-dithiolate ligand, the $dmit^{2-}$ ligand ($dmit^{2-}$ = 2-thioxo-1,3-dithiole-4,5-dithiolato).[15] Three of these superconducting salts, $(NMe_4)_{0.5}[Ni(dmit)_2]$,[16] β-$(NMe_4)_{0.5}[Pd(dmit)_2]$,[17] and $[NMe_2Et_2]_{0.5}[Pd(dmit)_2]$,[18] contain closed-shell cations, and four, $(TTF)[Ni(dmit)_2]_2$,[19] α- and α′-$(TTF)[Pd(dmit)_2]_2$,[20,21] and α-$(EDT\text{-}TTF)[Ni(dmit)_2]$,[22] contain open-shell cations.

With the aim of extending the range of conductors and possibly superconductors in this series, extensive studies have been carried out on $M(dmit)_2$-related systems obtained not only by changing the nature of the metal and the countercation[14,15] but also by using other ligands resembling $dmit^{2-}$, such as, for example, selenium-substituted $dmit^{2-}$ ligands,[23] 1,2,5-thiadiazole-3,4-dithiolato ($tdas^{2-}$),[24] and dimercaptobenzeneisotrithione ($dmbit^{2-}$).[25]

Along the same line, we report here on the synthesis and crystal structure of metal (Ni, Pd, Pt) complexes of two 1,2-dithiolate ligands resembling $dmit^{2-}$, the 5,6-dihydro-1,4-dithiin-2,3-dithiolato ($dddt^{2-}$) and 5,7-dihydro-1,4,6-trithiin-2,3-dithiolato ($dtdt^{2-}$) ligands. We also report on their electrochemical behavior compared to that of analogue complexes of the $dmit^{2-}$ ligand, the tentative preparation of their derived charge transfer salts, and the preparation, crystal and electronic structure, and conducting properties of new charge transfer salts of metal (Ni, Pd) complexes of the $dmit^{2-}$ ligand using PPN^+ [bis(triphenylphosphoranylidene)], BTP^+ (benzyltriphenylphosphonium), and the sulfonium cations of the $(SMe_yEt_{3-y})^+$ series with y = 0, 1, 2, and 3 as countercations.

Experimental Section

Syntheses. All syntheses were carried out by using vacuum line and Schlenk techniques in a dried N_2 atmosphere. The main starting dmit-based compounds, *e.g.*, $(NBu_4)_2[Zn(dmit)_2]$,[26] $dmit(COPh)_2$,[26] $dmitNa_2$,[27] and $(NR_4)[M(dmit)_2]$,[14] were prepared as previously described.

$(NR_4)[M(dddt)_2]$. These complexes (M = Ni, Pd, Pt) were obtained by hydrolysis of the $C_5H_4S_5$ thione (5,6-dihydro-1,3-dithiolo[4,5,6][1,4]-dithiin-2-thione),[27] affording the K_2dddt salt,[28,29] subsequent complexation with an appropriate metal salt, and precipitation with NR_4Br (R = Et, Bu), following previously reported procedures.[29−31] In the case of the nickel complex, a mixture of the divalent $(NBu_4)_2[Ni(dddt)_2]$ and monovalent $(NBu_4)[Ni(dddt)_2]$ complexes is obtained. Separation of these complexes by recrystallization failed, and oxidation by bubbling air through the reaction mixture for 15 min is required to obtain the pure monovalent salt. Only the monovalent $(NBu_4)[Pt(dddt)_2]$ and $(NEt_4)[Pd(dddt)_2]$ complexes can be obtained, even under N_2 atmosphere. The preparation of $(NEt_4)[Pd(dddt)_2]$ is difficult because of its instability in the generally used water/ethanol medium. This complex is best obtained when THF is used as solvent and bis(benzonitrile)dichloropalladium(II) $[(C_6H_5CN)_2PdCl_2]$[32] is used as the palladium source. Thus, the formation of metallic sulfides observed when K_2PdCl_4 or $PdCl_2$ is used in water/ethanol[30] may be avoided. The $(NR_4)[M(dddt)_2]$ complexes were recrystallized in acetone/2-propanol (1/1) and characterized by elemental analysis and infrared spectroscopy (supplementary material, Table S1).

$[M(dddt)_2]^0$.[33−35] The derived neutral complexes (M = Ni, Pt) were obtained[31] by chemical oxidation of the corresponding monovalent complexes by tetracyanoquinodimethane. They were characterized by elemental analysis and infrared spectroscopy (supplementary material, Table S1).

(5) Williams, J. M.; Schultz, A. J.; Underhill, A. E.; Carneiro, K. In *Extended Linear Chain Compounds*; Miller, J. S., Ed.; Plenum Press: New York, 1982; Vol. 1, pp 73−118.
(6) Reis, A. H., Jr. In *Extended Linear Chain Compounds*; Miller, J. S., Ed.; Plenum Press: New York, 1982; Vol. 1, pp 157−196.
(7) Marks, T. J.; Kalina, D. W. in *Extended Linear Chain Compounds*; Miller, J. S., Ed.; Plenum Press: New York, 1982; Vol. 1, pp 197−331.
(8) (a) Cassoux, P.; Interrante, L. V.; Kasper, J. *C.R. Acad. Sci. (Paris), Série C* **1980**, *291*, 25−28. (b) Cassoux, P.; Interrante, L. V.; Kasper, J. *Mol. Cryst. Liq. Cryst.* **1982**, *81*, 293.
(9) McLure, M. S.; Lin, L. S.; Whang, T. C.; Ratajack, M. T.; Kannewurf, C. R.; Marks, T. J. *Bull. Am. Phys. Soc.* **1980**, *25*, 314.
(10) Ibers, J. A.; Pace, L. J.; Martinsen, J.; Hoffman, B. M. *Struct. Bonding (Berlin)* **1982**, *50*, 1.
(11) Hünig, S.; Erk, P. *Adv. Mater.* **1991**, *3*, 225.
(12) Kobayashi, H.; Sawa, H.; Aonuma, S.; Kato, R. *J. Am. Chem. Soc.* **1993**, *115*, 7870.
(13) Cassoux, P.; Interrante, L. V. *Comments Inorg. Chem.* **1991**, *12*, 47.
(14) Cassoux, P.; Valade, L.; Kobayashi, H.; Kobayashi, A.; Clark, R. A.; Underhill, A. *Coord. Chem. Rev.* **1991**, *110*, 115.
(15) Cassoux, P.; Valade, L. in *Inorganic Materials*; Bruce, D. W., O'Hare, D., Eds.; J. Wiley & Sons: Chichester, England, 1992; pp 1−58.
(16) (a) Kobayashi, A.; Kim, H.; Sasaki, Y.; Kato, R.; Kobayashi, H.; Moriyama, S.; Nishio, Y.; Kajita, K.; Sasaki, W. *Chem. Lett.* **1987**, 1819. (b) Kajita, K.; Nishio, Y.; Moriyama, S.; Kato, R.; Kobayashi, H.; Sasaki, W. *Solid State Commun.* **1988**, *65*, 361.
(17) Kobayashi, A.; Kobayashi, H.; Miyamoto, A.; Kato, R.; Clark, R. A.; Underhill, A. E. *Chem. Lett.* **1991**, 2163.
(18) Kobayashi, H.; Bun, K.; Naito, T.; Kato, R.; Kobayashi, A. *Chem. Lett.* **1992**, 1909.
(19) (a) Brossard, L.; Ribault, M.; Bousseau, M.; Valade, L.; Cassoux, P. *C.R. Acad. Sci. (Paris), Série II* **1986**, *302*, 205. (b) Brossard, L.; Ribault, M.; Valade, L.; Cassoux, P. *Phys. B & C (Amsterdam)* **1986**, *143*, 378. (c) Bousseau, M.; Valade, L.; Legros, J.-P.; Cassoux, P.; Garbauskas, M.; Interrante, L. V. *J. Am. Chem. Soc.* **1986**, *108*, 1908.
(20) Brossard, L.; Ribault, M.; Valade, L.; Cassoux, P. *J. Phys. (Paris)* **1989**, *50*, 1521.
(21) Brossard, L.; Hurdequint, H.; Ribault, M.; Valade, L.; Legros, J.-P.; Cassoux, P. *Synth. Metals* **1988**, *27*, B157.
(22) Tajima, H.; Inokuchi, M.; Kobayashi, A.; Ohta, T.; Kato, R.; Kobayashi, H.; Kuroda, H. *Chem. Lett.* **1993**, 1235.
(23) (a) Cornelissen, J. P.; Haasnoot, J. G.; Reedijk, J.; Faulmann, C.; Legros, J.-P.; Cassoux, P.; Nigrey, P. *Inorg. Chim. Acta* **1992**, *202*, 131. (b) Olk, R.-M.; Kirmse, R.; Hoyer, E.; Faulmann, C.; Cassoux, P. *Z. Anorg. Allg. Chem.* **1994**, *620*, 90. (c) Naito, T.; Sato, A.; Kawano, K.; Taneto, A.; Kobayashi, H.; Kobayashi, A. *J. Chem. Soc., Chem. Commun.* **1995**, 351.
(24) Dyachenko, O. A.; Konovalikhin, S. V.; Kotov, A. I.; Shilov, G. V.; Yagubskii, E. B.; Faulmann, C.; Cassoux, P. *J. Chem. Soc., Chem. Commun.* **1993**, 508. (b) Awaga, K.; Okuno, T.; Maruyama, Y.; Kobayashi, A.; Kobayashi, H.; Schenk, S.; Underhill, A. E. *Inorg. Chem.* **1994**, *33*, 5598.
(25) Noh, D.-Y.; Mizuno, M.; Choy, J.-H. *Inorg. Chim. Acta* **1994**, *216*, 147.
(26) (a) Steimecke, G.; Sieler, H. J.; Kirmse, R.; Hoyer, E. *Phosphorus Sulfur* **1979**, *7*, 49. (b) Valade, L.; Legros, J.-P.; Bousseau, M.; Cassoux, P.; Garbauskas, M.; Interrante, L. V. *J. Chem. Soc., Dalton Trans.* **1985**, 783.
(27) Varma, K. S.; Bury, A.; Harris, N. J.; Underhill, A. E. *Synthesis* **1987**, *9*, 837.
(28) Vance, C. T.; Bereman, R. D.; Bordner, J.; Hatfield, W. E.; Helms, J. H. *Inorg. Chem.* **1985**, *24*, 2905.
(29) Kato, R.; Kobayashi, H.; Kobayashi, A.; Sasaki, Y. *Bull. Chem. Soc. Jpn.* **1986**, *59*, 627.
(30) Vance, C. T.; Bereman, R. D. *Inorg. Chim. Acta* **1988**, *149*, 229.
(31) Detailed synthetic procedures may be found in Errami, A. E. Conducteurs Moléculaires Dérivés de Complexes Métalliques à Ligands 1,2-Dithiolates Polysoufrés. Ph.D. Thesis, University of Toulouse, Toulouse, France, March 27, 1995.
(32) Kharasch, M. S.; Seyler, R. C.; Mayo, F. R. *J. Chem. Soc.* **1938**, *60*, 882.
(33) Nahapetyan, S. S.; Shklover, V. E.; Vetoshkina, L. V.; Kotov, A. I.; Ukhin, L. Yu.; Struchkov, Yu. T.; Yagubskii E. B. *Mater. Sci.* **1988**, *14*, 5.
(34) Kim, H.; Kobayashi, A.; Sasaki, Y.; Kato, R.; Kobayashi, H. *Bull. Chem. Soc. Jpn.* **1988**, *61*, 579.
(35) Gritsenko, V. V.; Dyachenko, O. A.; Cassoux, P.; Kotov, A. I.; Laukhina, E. E.; Faulmann, C.; Yagubskii, E. B. *Russ. Chem. Bull.* **1993**, *42*, 1149.

Table 1. Crystallographic Data for $(NBu_4)[Pt(dtdt)_2]$ (**1**), $(PPN)[Ni(dmit)_2]\cdot(CH_3)_2CO$ (**2**), $(SMeEt_2)[Ni(dmit)_2]$ (**3**), $[Pt(dddt)_2][Ni(dmit)_2]_2$ (**4**), $(BTP)[Ni(dmit)_2]_3$ (**5**), $(SMe_3)[Ni(dmit)_2]_2$ (**6**), and $(SMeEt_2)[Pd(dmit)_2]_2$ (**7**)

	compound						
	1	**2**	**3**	**4**	**5**	**6**	**7**
chem formula	$C_{24}H_{44}NPtS_{10}$	$C_{45}H_{36}NNiS_{10}P_2O$	$C_{11}H_{13}NiS_{11}$	$C_{20}H_8Ni_2PtS_{28}$	$C_{43}H_{22}PNi_3S_{30}$	$C_{15}H_9Ni_2S_{21}$	$C_{17}H_{13}Pd_2S_{21}$
fw	862.3	1048.0	556.6	1458.5	1707.5	971.9	1103.4
space group	$P2_1/n$	$P\bar{1}$	$P2_1/n$	$C2/m$	$P\bar{1}$	$P\bar{1}$	$P\bar{1}$
a (Å)	12.064(2)	12.310(2)	7.171(9)	20.336(4)	11.927(2)	7.882(1)	7.804(4)
b (Å)	17.201(3)	13.328(3)	17.802(3)	7.189(2)	24.919(2)	11.603(2)	36.171(18)
c (Å)	16.878(2)	15.850(3)	16.251(3)	14.181(2)	11.829(3)	17.731(2)	6.284(2)
α (deg)		108.19(3)			93.11(1)	77.44(1)	91.68(4)
β (deg)	102.22(2)	96.64(2)	94.39(4)	97.16(2)	110.22(1)	94.39(1)	112.08(4)
γ (deg)		99.67(2)			83.94(1)	81.27(1)	88.79(5)
V (Å^3)	3423(1)	2373(1)	2068(2)	2057(1)	3284(1)	1563(1)	1643(1)
ρ_{calcd} (g cm^{-3})	1.674	1.367	1.788	2.36	1.73	2.08	2.23
Z	4	2	4	2	2	2	2
μ(Mo Kα) (cm^{-1})	47.5	9.3	20.1	57.3	18.3	25.7	23.8
$R(F_o)^a$	0.031	0.057	0.031	0.047	0.049	0.075	0.074
$R_w(F_o)^a$	0.035	0.068	0.033	0.049	0.051	0.084	0.079

[a] $R(F_o) = \sum(||F_o| - |F_c||)/\sum|F_o|$ and $R_w(F_o) = [\sum w(|F_o| - |F_c|)^2/\sum wF_o^2]^{1/2}$.

$(NR_4)[M(dtdt)_2]$. These complexes (M = Ni, Pd, Pt) were obtained by following a method, similar to that used for the $(NR_4)_2[Ni(dddt)_2]$ complexes, based on the hydrolysis of the $C_5H_4S_6$ thione (1,3-[4,5-*f*]-[1,3,5]trithiepin-2-thione),[36] affording the K_2dtdt salt, and subsequent metal complexation.

$(NMe_4)[Ni(dtdt)_2]$. Recrystallization of this complex, obtained as in ref 29 and precipitated by using NMe_4Br instead of NBu_4Br, succeeded in a mixture of acetone/2-propanol (1/1).

$(NBu_4)[Pt(dtdt)_2]$ (1). $C_5H_4S_6$ (1 g, 3.9 mmol) was treated with 2 g (36 mmol) of KOH in 20 mL of ethanol. The solution was stirred at 50 °C for 1.5 h. The mixture was cooled down to room temperature and filtered, and the pale yellow crystals of K_2dtdt were washed with ethanol (three portions of 4 mL) and dried under vacuum. The K_2dtdt salt was dissolved in 40 mL of a water/ethanol (1/1) mixture and treated dropwise with 0.8 g (1.9 mmol) of K_2PtCl_4 in 30 mL of water. After 30 min of stirring, 0.7 g (2.2 mmol) of NBu_4Br in 20 mL of water was added to the solution. The dark green precipitate was isolated by filtration, washed with ethanol, and dried under vacuum. Recrystallization in acetone/2-propanol (1/1) afforded 0.50 g of dark green crystals.

$(NBu_4)[Pd(dtdt)_2]$. The K_2dtdt salt obtained as in the preceding paragraph was dissolved in 100 mL of THF and treated dropwise with 0.75 g (1.95 mmol) of $(C_6H_5CN)_2PdCl_2$ in 50 mL of THF. The brown mixture turned dark green during the addition. The solution was stirred for an additional 30 min. NBu_4Br (0.63 g, 1.95 mmol) in 50 mL of water was then added dropwise. After concentration of the solution with a rotary evaporator and filtration, a brown green precipitate was obtained, which was washed with 20 mL of methanol. Recrystallization in a mixture of acetone/2-propanol (1/1) afforded 0.40 g of brown green crystals.

These $(NR_4)[M(dtdt)_2]$ complexes were characterized by elemental analysis and infrared spectroscopy (supplementary material, Table S1). The $(NBu_4)[Pt(dtdt)_2]$ complex (**1**) was further characterized by X-ray crystal structure determination (*vide infra*).

$(cation)_2[M(dmit)_2]$ (M = Ni, Pd). The cations used in this work were PPN^+ [bis(triphenylphosphoranylidene)], BTP^+ (benzyltriphenylphosphonium), and the sulfonium cations of the $(SMe_yEt_{3-y})^+$ series with $y = 0$, 1, 2, and 3. The $(cation)_2[M(dmit)_2]$ divalent complexes were prepared by the now standard one-pot method,[14,26] involving generation of the $dmit^{2-}$ ligand in a methanol solution by reaction of $dmit(COPh)_2$ with methanolate, reaction of an appropriate metal salt ($NiCl_2\cdot6H_2O$ or Na_2PdCl_4, respectively), and precipitation in the final step of the desired $(cation)_2[M(dmit)_2]$ complex by addition of the chloride of the appropriate cation.[31] All complexes were recrystallized in acetone/2-propanol (1/1) and characterized by elemental analysis and infrared spectroscopy (supplementary material, Table S1).

$(cation)[M(dmit)_2]$. These monovalent complexes (M = Ni and the same cations as before; M = Pd and cation = PPN^+ and BTP^+) were obtained from the corresponding divalent $(cation)_2[M(dmit)_2]$ complexes by oxidation with I_2/NaI.[14,26,31] All complexes were recrystallized in acetone/2-propanol (1/1) and characterized by elemental analysis and infrared spectroscopy (supplementary material, Table S1). $(PPN)[Ni(dmit)_2]\cdot(CH_3)_2CO$ (**2**) and $(SMeEt_2)[Ni(dmit)_2]$ (**3**) were further characterized by determination of their crystal structures by X-ray diffraction methods (*vide infra*). In the series of palladium complexes with the cation $(SMe_yEt_{3-y})^+$, iodine oxidation of the divalent $(SMe_yEt_{3-y})_2[Pd(dmit)_2]$ complexes leads to the formation of insoluble solids [probably noninteger oxidation state (NIOS) compounds of the type $(SMe_yEt_{3-y})[Pd(dmit)_2]_z$], and the corresponding monovalent $(SMe_yEt_{3-y})[Pd(dmit)_2]$ complexes could not be isolated. This is related to the redox properties of these systems (*vide infra*).

Electrocrystallization. $[M(dddt)_2][M'(dmit)_2]_x$ complexes (M = Ni, Pt; M′ = Ni, Pd) have been prepared by galvanostatic (1−6 μA/cm^2) electrochemical oxidation on a platinum electrode from solutions of $[M(dddt)_2]^0$ and $(NBu_4)[M'(dmit)_2]$ in an appropriate solvent and characterized by elemental analysis (supplementary material, Table S2). $[Pt(dddt)_2][Ni(dmit)_2]_2$ (**4**) was further characterized by determination of its crystal structure by X-ray diffraction methods (*vide infra*). Likewise, the $(cation)[M(dmit)_2]_z$ NIOS salts were obtained by galvanostatic (1−3 μA/cm^2) electrochemical oxidation of solutions of the appropriate monovalent [or divalent in the case of the $(SMe_yEt_{3-y})_2[Pd(dmit)_2]$ series] complexes, following previously reported procedures,[15] and characterized by elemental analysis (supplementary material, Tables S3 and S4). Compounds $(BTP)[Ni(dmit)_2]_3$ (**5**), $(SMe_3)[Ni(dmit)_2]_2$ (**6**), and $(SMeEt_2)[Pd(dmit)_2]_2$ (**7**) were further characterized by determination of their crystal structures by X-ray diffraction methods (*vide infra*).

Electrochemical Studies. Slow (v < 1 V s^{-1}) and fast (v > 1 V s^{-1} and up to 1000 V.s^{-1}) voltammetric measurements and controlled potential electrolysis were carried out with an ISMP Model Elektromat 400 microcomputer-controlled instrumentation with positive feedback ohmic resistance compensation,[37] following previously described techniques.[38,39]

X-ray Diffraction Data Collection and Structure Determination. All data were collected at room temperature on an Enraf-Nonius CAD4 diffractometer with graphite-monochromated Mo Kα radiation (λ = 0.710 73 Å) by using the CAD4-Express package.[40] For every compound, the intensity of three reflections was monitored throughout the data collection, and no significant decay was observed. Accurate unit cell parameters were obtained by least-squares refinements on the basis of the setting angles of 25 reflections, unless otherwise specified. Crystallographic data for $(NBu_4)[Pt(dtdt)_2]$ (**1**), $(PPN)[Ni(dmit)_2]\cdot(CH_3)_2CO$ (**2**), $(SMeEt_2)[Ni(dmit)_2]$ (**3**), $[Pt(dddt)_2][Ni(dmit)_2]_2$ (**4**), (BTP)-

(36) Russkikh, V. S.; Abashev, G. G. *Khim. Geterotsikl. Soedin* **1987**, *11*, 1483.

(37) Cassoux, P.; Dartiguepeyron, R.; David, C.; de Montauzon, D.; Tommasino, J.-B.; Fabre, P.-L. *L'Actual. Chim.* **1994**, *1*−2, 49.

(38) Tommasino, J.-B.; Pomarede, B.; Medus, D.; de Montauzon, D.; Cassoux, P. *Mol. Cryst. Liq. Cryst.* **1993**, *237*, 445.

(39) Faulmann, C.; Cassoux, P.; Yagubskii, E. B.; Vetoshkina, L. V. *New J. Chem.* **1993**, *17*, 385.

(40) Enraf-Nonius, CAD4-Express, version 5.1, Delft, Holland, 1992.

Table 2. Atomic Parameters for $(NBu_4)[Pt(dtdt)_2]$ (**1**)

atom	*x*/*a*	*y*/*b*	*z*/*c*	U_{eq}[a] (Å^2)
Pt(1)	0.14950(3)	0.86428(2)	0.86803(3)	0.0404
S(1)	0.0381(2)	0.7577(2)	0.8609(2)	0.0529
S(2)	0.2434(2)	0.8236(2)	0.9913(2)	0.0493
S(3)	0.0115(2)	0.6259(2)	0.9646(2)	0.0597
S(4)	0.2326(3)	0.6928(2)	1.1009(2)	0.0565
S(5)	0.2039(3)	0.5205(2)	1.0516(2)	0.0677
S(6)	0.2700(2)	0.9657(2)	0.8690(2)	0.0481
S(7)	0.0538(2)	0.9038(2)	0.7451(2)	0.0575
S(8)	0.3184(2)	1.0778(2)	0.7486(2)	0.0550
S(9)	0.0891(3)	1.0127(2)	0.6199(2)	0.0685
S(10)	0.1445(3)	0.1866(2)	0.6457(2)	0.0757
N(1)	0.3278(6)	0.0810(4)	0.1355(5)	0.0413
C(1)	0.0867(8)	0.7104(6)	0.9508(6)	0.0479
C(2)	0.1771(8)	0.7389(6)	1.0076(6)	0.0455
C(3)	0.1113(9)	0.5486(6)	0.9594(6)	0.0479
C(4)	0.2927(9)	0.6047(7)	1.0702(7)	0.0613
C(5)	0.1349(9)	0.9790(6)	0.7209(6)	0.0516
C(6)	0.2285(8)	1.1097(8)	0.6367(8)	0.0770
C(7)	0.042(1)	1.1097(8)	0.6367(8)	0.0770
C(8)	0.234(1)	0.1657(6)	0.7413(7)	0.0626
C(9)	0.3825(8)	1.1279(6)	0.2087(6)	0.0483
C(10)	0.5052(9)	0.1094(6)	0.2475(6)	0.0532
C(11)	0.5487(9)	0.1682(7)	0.3134(6)	0.0540
C(12)	0.671(1)	0.1546(8)	0.3552(8)	0.0742
C(13)	0.3345(8)	−0.0058(5)	0.1539(6)	0.0447
C(14)	0.2808(9)	−0.0345(6)	0.2204(6)	0.0530
C(15)	0.308(1)	−0.1199(7)	0.2363(7)	0.0684
C(16)	0.245(1)	−0.1574(8)	0.2928(8)	0.0733
C(17)	0.3885(9)	0.0916(7)	0.0660(6)	0.0494
C(18)	0.404(1)	0.1742(8)	0.0415(7)	0.0656
C(19)	0.440(1)	0.1755(9)	−0.0388(7)	0.0748
C(20)	0.465(1)	0.254(1)	−0.0681(9)	0.0824
C(21)	0.2045(9)	0.1073(6)	0.1127(7)	0.0560
C(22)	0.132(1)	0.0760(7)	0.0347(8)	0.0680
C(23)	0.105(1)	0.1324(9)	0.0324(8)	0.0889
C(24)	0.014(1)	0.1074(8)	−0.1021(8)	0.0756

[a] $U_{eq} = {}^1/_3\sum_i\sum_j U_{ij}a_i^*a_j^*\mathbf{a}_i\mathbf{a}_j$.

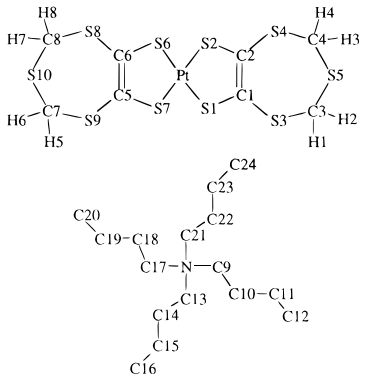

Figure 1. Atomic numbering scheme for $(NBu_4)[Pt(dtdt)_2]$ (**1**).

$[Ni(dmit)_2]_3$ (**5**), $(SMe_3)[Ni(dmit)_2]_2$ (**6**), and $(SMeEt_2)[Pd(dmit)_2]_2$ (**7**) are summarized in Table 1. All calculations were performed by using a Gateway 2000 personal computer with the Crystals package.[41] Final atom positional and equivalent thermal parameters are listed in Tables 2−8. Additional relevant parameters of data collections and refinements and the anisotropic thermal parameters are given in the supplementary material (Tables S5−S25). The atomic numbering schemes are shown in Figures 1−5. The atomic scattering factors used were those calculated by Cromer and Waber.[42] The positions of the metal atoms and most of the sulfur atoms were determined by direct methods using Shelxs-86.[43] The remaining non-hydrogen atoms were located from subsequent difference Fourier maps. The positions of the hydrogen atoms were calculated and not refined unless otherwise specified, and their contribution was included in the calculations by using an isotropic displacement parameter, $B = 1.3B_{iso}$C atom) Å^2. Absorption correction based on DIFABS[44] was applied to each data set.

Table 3. Atomic Parameters for $(PPN)[Ni(dmit)_2]\cdot(CH_3)_2CO]$ (**2**)

atom	*x*/*a*	*y*/*b*	*z*/*c*	U_{eq}[a]/U_{iso} (Å^2)
Ni(1)	0.48375(8)	0.09063(8)	0.34413(7)	0.0405
S(1)	0.3206(2)	0.1106(2)	0.2936(1)	0.0495
S(2)	0.4436(2)	0.1050(2)	0.4760(1)	0.0503
S(3)	0.1184(2)	0.1433(2)	0.3830(1)	0.0558
S(4)	0.2312(2)	0.1361(2)	0.5506(1)	0.0557
S(5)	0.0005(2)	0.1745(3)	0.5400(2)	0.0796
S(6)	0.6428(2)	0.0616(2)	0.3929(1)	0.0497
S(7)	0.5284(2)	0.0869(2)	0.2151(1)	0.0502
S(8)	0.8434(2)	0.0226(2)	0.3020(2)	0.0562
S(9)	0.7389(2)	0.0489(2)	0.1401(1)	0.0578
S(10)	0.9686(2)	0.0084(2)	0.1506(2)	0.0736
N(1)	0.3721(5)	0.6138(4)	0.8341(4)	0.0391
P(1)	0.2433(2)	0.5980(1)	0.8352(1)	0.0367
P(2)	0.4541(2)	0.5531(2)	0.7760(1)	0.0371
C(1)	0.2548(7)	0.1244(6)	0.3846(5)	0.0460
C(2)	0.3084(6)	0.1218(6)	0.4637(5)	0.0441
C(3)	0.1108(7)	0.1528(7)	0.4945(6)	0.0534
C(4)	0.7099(7)	0.0494(6)	0.3018(6)	0.0443
C(5)	0.6584(6)	0.0599(5)	0.2246(5)	0.0408
C(6)	0.8563(7)	0.0257(6)	0.1949(6)	0.0541
C(7)	0.1609(6)	0.6012(6)	0.7351(5)	0.036(2)
C(8)	0.2055(6)	0.6670(6)	0.6907(5)	0.043(2)
C(9)	0.1424(7)	0.6770(7)	0.6169(6)	0.055(2)
C(10)	0.0333(7)	0.6222(7)	0.5895(6)	0.060(2)
C(11)	−0.0131(8)	0.5665(7)	0.6336(6)	0.065(2)
C(12)	0.0491(7)	0.5440(7)	0.7056(6)	0.053(2)
C(13)	0.1872(6)	0.4760(6)	0.8554(5)	0.045(2)
C(14)	0.1607(7)	0.3772(7)	0.7855(6)	0.057(2)
C(15)	0.1319(9)	0.2816(9)	0.8040(7)	0.080(3)
C(16)	0.133(1)	0.286(1)	0.8903(9)	0.110(4)
C(17)	0.159(1)	0.381(1)	0.9603(9)	0.114(4)
C(18)	0.1855(9)	0.4790(9)	0.9420(7)	0.081(3)
C(19)	0.2244(6)	0.7089(5)	0.9271(5)	0.036(2)
C(20)	0.3149(7)	0.7732(7)	0.9932(6)	0.054(2)
C(21)	0.2992(8)	0.8578(8)	1.0646(6)	0.069(3)
C(22)	0.1962(7)	0.8802(7)	1.0682(6)	0.060(2)
C(23)	0.1070(8)	0.8203(8)	1.0038(6)	0.067(2)
C(24)	0.1204(7)	0.7322(7)	0.9321(6)	0.059(2)
C(25)	0.4174(6)	0.5312(5)	0.6577(4)	0.034(2)
C(26)	0.4605(6)	0.6113(6)	0.6247(5)	0.045(1)
C(27)	0.4196(7)	0.6044(7)	0.5367(6)	0.057(2)
C(28)	0.3353(7)	0.5194(7)	0.4837(6)	0.062(2)
C(29)	0.2933(7)	0.4384(7)	0.5159(6)	0.060(2)
C(30)	0.3326(6)	0.4449(6)	0.6030(5)	0.045(2)
C(31)	0.4606(6)	0.4248(6)	0.7896(5)	0.044(2)
C(32)	0.4448(7)	0.4150(7)	0.8723(6)	0.062(2)
C(33)	0.4458(9)	0.3174(9)	0.8866(7)	0.083(3)
C(34)	0.4656(9)	0.2325(9)	0.8187(7)	0.082(3)
C(35)	0.4833(8)	0.2417(8)	0.7392(7)	0.073(3)
C(36)	0.4811(7)	0.3384(7)	0.7235(5)	0.052(2)
C(37)	0.5918(6)	0.6374(6)	0.8142(5)	0.043(2)
C(38)	0.6088(6)	0.7408(6)	0.8780(5)	0.049(2)
C(39)	0.7178(8)	0.8044(7)	0.9058(6)	0.063(2)
C(40)	0.8026(8)	0.7696(8)	0.8707(6)	0.067(2)
C(41)	0.7879(8)	0.6682(8)	0.8084(6)	0.071(3)
C(42)	0.6815(7)	0.6001(7)	0.7813(6)	0.061(2)
C(43)	0.210(1)	0.692(1)	0.2889(8)	0.089(3)
C(44)	0.234(2)	0.807(2)	0.335(1)	0.184(7)
C(45)	0.183(1)	0.656(1)	0.196(1)	0.163(6)
O(1)	0.219(1)	0.628(1)	0.3226(9)	0.1584

[a] $U_{eq} = {}^1/_3\sum_i\sum_j U_{ij}a_i^*a_j^*\mathbf{a}_i\mathbf{a}_j$.

$(NBu_4)[Pt(dtdt)_2]$ (1). A block-shaped crystal of dimensions 0.2 × 0.2 × 0.4 mm^3 was used. Intensity data (6004 unique reflections with $h = 0-14$, $k = 0-20$, $l = -20$ to 20) were collected by the $\omega/1.3\theta$ scan technique in the θ range 1.5−25°. Reflections (2977) with $I > 3\sigma(I)$ were used in the calculations. Full matrix least-squares refinement

(41) Watkin, D. J.; Carruthers, J. R.; Betteridge, P. W. *CRYSTALS User guide*; Chemical Crystallography Laboratory: University of Oxford, Oxford, UK, 1985.
(42) Cromer, D. T.; Waber, J. T. *International Tables for X-Ray Crystallography*; Kynoch Press: Birmingham, England, 1974; Vol. IV, Table 2.2B, p 99.
(43) Sheldrick, G. M. *SHELXS86, Program for Crystal Structure Solution*; University of Göttingen: Göttingen, Germany, 1986.
(44) Walker, N.; Stuart, D. *Acta Crystallogr.* **1983**, *A39*, 158.

Table 4. Atomic Parameters for $(SMeEt_2)[Ni(dmit)_2]$ (**3**)

atom	*x*/*a*	*y*/*b*	*z*/*c*	U_{eq}[a] (Å^2)
Ni(1)	0.2576(1)	0.02625(5)	0.55522(5)	0.0420
S(1)	0.2888(3)	0.1110(1)	0.6515(1)	0.0513
S(2)	0.2569(2)	0.1081(1)	0.4573(1)	0.0488
S(3)	0.3057(2)	0.2816(1)	0.6387(1)	0.0525
S(4)	0.2814(2)	0.2773(1)	0.4617(1)	0.0512
S(5)	0.3128(3)	0.4255(1)	0.5449(1)	0.0657
S(6)	0.2368(3)	−0.0556(1)	0.4574(1)	0.0527
S(7)	0.2517(2)	−0.0593(1)	0.6502(1)	0.0480
S(8)	0.2173(3)	−0.2252(1)	0.4603(1)	0.0524
S(9)	0.2280(3)	−0.2295(1)	0.6373(1)	0.0537
S(10)	0.2156(3)	−0.3731(1)	0.5432(1)	0.0669
S(11)	0.2946(2)	0.0104(1)	0.2458(1)	0.0530
C(2)	0.2760(8)	0.1907(4)	0.5114(4)	0.0391
C(3)	0.2997(8)	0.3334(4)	0.5482(4)	0.0476
C(4)	0.2312(8)	−0.1388(4)	0.5095(4)	0.0433
C(5)	0.2370(8)	−0.1402(4)	0.5936(4)	0.0404
C(6)	0.2200(8)	−0.2816(4)	0.5465(4)	0.0478
C(7)	0.100(1)	−0.0539(4)	0.2159(6)	0.0710
C(8)	0.159(1)	−0.1322(5)	0.2352(5)	0.0795
C(9)	0.184(1)	0.0985(4)	0.2213(5)	0.0680
C(10)	0.317(1)	0.1630(5)	0.2354(6)	0.0732
C(11)	0.445(1)	−0.0024(5)	0.1635(5)	0.0757

[a] $U_{eq} = {}^1/_3\sum_i\sum_j U_{ij}a_i^*a_j^*\mathbf{a}_i\mathbf{a}_j$.

Table 5. Atomic Parameters for $[Pt(dddt)_2][Ni(dmit)_2]_2$ (**4**)

atom	*x*/*a*	*y*/*b*	*z*/*c*	U_{eq}[a] (Å^2)
Pt(1)	0.0000	0.0000	0.0000	0.0214
Ni(1)	0.27953(8)	0.0000	0.9673(1)	0.0216
S(1)	0.3766(2)	0.0000	0.9237(3)	0.0354
S(2)	0.2316(2)	0.0000	0.8244(3)	0.0362
S(3)	0.4219(2)	0.0000	0.7309(3)	0.0434
S(4)	0.2870(2)	0.0000	0.6373(3)	0.0469
S(5)	0.3991(3)	0.0000	0.5221(4)	0.0610
S(6)	0.1828(2)	0.0000	1.0098(3)	0.0360
S(7)	0.3267(2)	0.0000	1.1104(3)	0.0351
S(8)	0.1365(2)	0.0000	1.2036(3)	0.0333
S(9)	0.2713(2)	0.0000	1.2971(3)	0.0422
S(10)	0.1594(3)	0.0000	1.4116(3)	0.0517
S(11)	−0.0225(1)	−0.2166(4)	0.1053(2)	0.0298
S(12)	−0.0683(2)	−0.2376(4)	0.2890(2)	0.0388
C(1)	0.3600(8)	0.0000	0.805(1)	0.0294
C(2)	0.2957(8)	0.0000	0.760(1)	0.0340
C(3)	0.3715(8)	0.0000	0.623(1)	0.0397
C(4)	0.1979(8)	0.0000	1.126(1)	0.0309
C(5)	0.2640(7)	0.0000	1.175(1)	0.0254
C(6)	0.1869(7)	0.0000	1.311(1)	0.0342
C(7)	−0.0451(4)	−0.0981(1)	0.1984(6)	0.0219
C(8)[b]	−0.047(1)	−0.102(4)	0.392(2)	0.0397
C(9)[b]	−0.087(2)	−0.1084(4)	0.385(2)	0.0248

[a] $U_{eq} = {}^1/_3\sum_i\sum_j U_{ij}a_i^*a_j^*\mathbf{a}_i\mathbf{a}_j$. [b] Structure occupation factor, 0.5.

in the space group $P2_1/n$ with all non-hydrogen atoms anisotropic and the H atoms of the anion isotropic and refined gave $R = 0.031$ and $R_w = 0.035$.

$(PPN)[Ni(dmit)_2]\cdot(CH_3)_2CO$ (2). A black platelet of dimensions $0.38 \times 0.18 \times 0.05$ mm^3 was used. Intensity data (5830 unique reflections with $h = -12$ to 12, $k = -14$ to 14, $l = 0-16$) were collected by the ω/θ scan technique in the θ range 2.2−22°. Reflections (3589) with $I > 3\sigma(I)$ were used in the calculations. All non-hydrogen atoms, except those belonging to the phenyl groups, were refined anisotropically in the space group $P\bar{1}$. The final R values were $R = 0.057$ and $R_w = 0.068$.

$(SMeEt_2)[Ni(dmit)_2]$ (3). A needle-shaped crystal of dimensions $0.09 \times 0.23 \times 0.40$ mm^3 was used. Intensity data (3642 unique reflections with $h = 0-8$, $k = 0-21$, $l = -19$ to 19) were collected by the $\omega/2\theta$ scan technique in the θ range 1.5−25°. Reflections (1972) with $I > 3\sigma(I)$ were used in the calculations. All non-hydrogen atoms were refined anisotropically in the space group $P2_1/n$. The final R values were $R = 0.031$ and $R_w = 0.033$.

$[Pt(dddt)_2][Ni(dmit)_2]_2$ (4). A needle-shaped crystal of dimensions $0.10 \times 0.15 \times 0.37$ mm^3 was used. Intensity data (1952 unique reflections with $h = 0-24$, $k = 0-8$, $l = -16$ to 16) were collected by the ω scan technique in the θ range 2−25°. Reflections (1302) with $I > 3\sigma(I)$ were used in the calculations. All non-hydrogen atoms

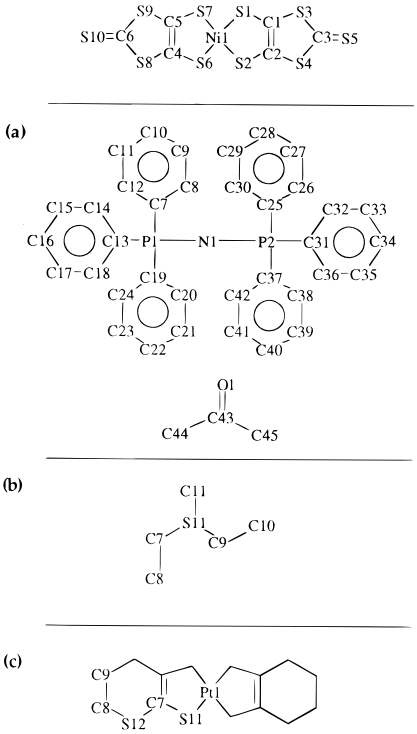

Figure 2. Atomic numbering scheme for (a) $(PPN)[Ni(dmit)_2]\cdot(CH_3)_2CO$ (**2**), (b) $(SMeEt)_2[Ni(dmit)_2]$ (**3**), and (c) $[Pt(dddt)_2][Ni(dmit)_2]_2$ (**4**).

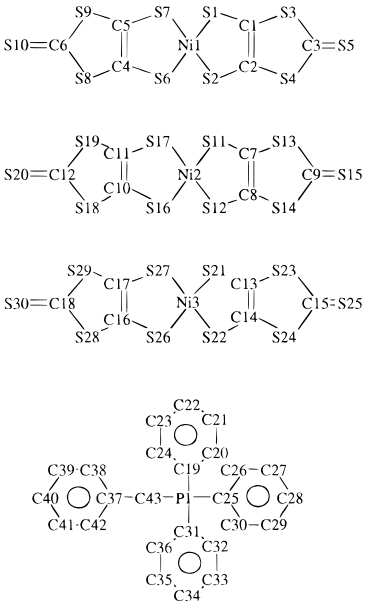

Figure 3. Atomic numbering scheme for $(BTP)[Ni(dmit)_2]_3$ (**5**).

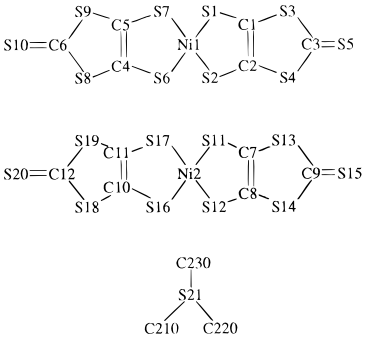

Figure 4. Atomic numbering scheme for $(SMe_3)[Ni(dmit)_2]_2$ (**6**).

Table 6. Atomic Parameters for (BTP)[Ni(dmit)$_2$]$_3$ (**5**)

atom	*x*/*a*	*y*/*b*	*z*/*c*	U_{eq}[a]/U_{iso} (Å^2)	atom	*x*/*a*	*y*/*b*	*z*/*c*	U_{eq}[a]/U_{iso} (Å^2)
Ni(1)	0.70354(7)	0.06141(3)	0.50133(7)	0.0304	C(6)	0.5301(7)	0.2732(3)	0.5029(7)	0.053(2)
Ni(2)	0.46091(7)	0.94411(3)	0.82461(7)	0.0293	C(7)	0.5131(6)	0.8232(3)	0.8526(6)	0.035(2)
Ni(3)	0.03769(7)	0.05518(3)	0.17199(7)	0.0287	C(8)	0.5905(6)	0.8360(3)	0.7953(6)	0.033(2)
S(1)	0.6609(2)	−0.01084(7)	0.5635(2)	0.0361	C(9)	0.6419(7)	0.7329(3)	0.8382(&)	0.049(2)
S(2)	0.8353(2)	0.01757(7)	0.4352(2)	0.0365	C(10)	0.4094(6)	1.0652(3)	0.8043(6)	0.034(2)
S(3)	0.7576(2)	−0.12759(7)	0.5571(2)	0.0404	C(11)	0.3346(6)	1.0513(3)	0.8639(6)	0.032(2)
S(4)	0.9169(2)	−0.10159(8)	0.4342(2)	0.0399	C(12)	0.2950(6)	1.1560(3)	0.8418(6)	0.040(2)
S(5)	0.9165(2)	−0.21528(9)	0.4967(2)	0.0625	C(13)	0.0941(6)	−0.0656(3)	0.1918(6)	0.038(2)
S(6)	0.7487(2)	0.13460(8)	0.4437(2)	0.0409	C(14)	0.1696(6)	−0.0500(3)	0.1333(6)	0.034(2)
S(7)	0.5687(2)	0.10414(7)	0.5659(2)	0.0378	C(15)	0.2144(7)	−0.1550(3)	0.1552(7)	0.047(2)
S(8)	0.6454(2)	0.25069(8)	0.4493(2)	0.0546	C(16)	-0.0151(6)	0.1756(3)	0.1503(6)	0.039(2)
S(9)	0.4801(2)	0.22254(8)	0.5618(2)	0.0479	C(17)	-0.0939(6)	0.1621(3)	0.2027(6)	0.037(2)
S(10)	0.4748(3)	0.33656(9)	0.4969(2)	0.0712	C(18)	-0.1412(7)	0.2648(3)	0.1695(7)	0.053(2)
S(11)	0.4185(2)	0.87176(7)	0.8871(2)	0.0387	C(19)	0.2279(7)	0.5236(3)	0.0840(7)	0.050(2)
S(12)	0.5937(2)	0.90106(7)	0.7591(2)	0.0354	C(20)	0.1809(9)	0.4792(4)	0.108(1)	0.068(3)
S(13)	0.5215(2)	0.75570(7)	0.8865(2)	0.0462	C(21)	0.1184(9)	0.4457(4)	0.015(1)	0.073(3)
S(14)	0.6880(2)	0.78307(8)	0.7735(2)	0.0460	C(22)	0.103(1)	0.4573(5)	−0.097(1)	0.082(3)
S(15)	0.7023(3)	0.67053(9)	0.8507(3)	0.0688	C(23)	0.144(1)	0.5014(5)	−0.127(1)	0.088(3)
S(16)	0.5020(2)	0.01749(7)	0.7644(2)	0.0355	C(24)	0.2087(9)	0.5349(4)	−0.0355(9)	0.069(3)
S(17)	0.3325(2)	0.98636(7)	0.8956(2)	0.0365	C(25)	0.1980(7)	0.6186(3)	0.2324(7)	0.046(2)
S(18)	0.4030(2)	1.13363(7)	0.7776(2)	0.0415	C(26)	0.1174(8)	0.6484(4)	0.1380(9)	0.060(2)
S(19)	0.2472(2)	1.10430(8)	0.9014(2)	0.0397	C(27)	0.0344(9)	0.6897(4)	0.162(1)	0.068(3)
S(20)	0.2430(2)	1.21887(9)	0.8447(2)	0.0604	C(28)	0.035(1)	0.6974(5)	0.275(1)	0.079(3)
S(21)	0.0006(2)	−0.01882(7)	0.2321(2)	0.0365	C(29)	0.114(1)	0.6682(5)	0.370(1)	0.087(3)
S(22)	0.1693(2)	0.01496(7)	0.1029(2)	0.0349	C(30)	0.197(1)	0.6277(4)	0.347(1)	0.077(3)
S(23)	0.1039(2)	−0.13379(7)	0.2182(2)	0.0442	C(31)	0.4100(7)	0.6004(3)	0.1561(7)	0.044(2)
S(24)	0.2612(2)	−0.10159(7)	0.0977(2)	0.0415	C(32)	0.4242(7)	0.6545(3)	0.1834(7)	0.050(2)
S(25)	0.2693(2)	−0.21647(9)	0.1505(2)	0.0627	C(33)	0.5119(8)	0.6775(4)	0.1532(9)	0.066(2)
S(26)	0.0789(2)	0.12814(7)	0.1122(2)	0.0371	C(34)	0.5834(9)	0.6479(4)	0.1004(9)	0.073(3)
S(27)	-0.0952(2)	0.09659(7)	0.2371(2)	0.0349	C(35)	0.5675(9)	0.5942(4)	0.0699(9)	0.072(3)
S(28)	-0.0217(2)	0.2463(8)	0.1219(2)	0.0495	C(36)	0.4822(8)	0.5700(4)	0.1011(8)	0.062(2)
S(29)	-0.1909(2)	0.21405(8)	0.2286(2)	0.0488	C(37)	0.4956(7)	0.4974(3)	0.3363(7)	0.052(2)
S(30)	-0.2018(3)	0.3269(1)	0.1611(3)	0.0823	C(38)	0.6053(9)	0.5172(4)	0.3788(9)	0.067(2)
P(1)	0.3054(2)	0.56879(8)	0.2016(2)	0.0466	C(39)	0.707(1)	0.4857(4)	0.378(1)	0.075(3)
C(1)	0.7527(6)	−0.0602(3)	0.5258(6)	0.032(2)	C(40)	0.700(1)	0.4342(5)	0.335(1)	0.082(3)
C(2)	0.8297(6)	−0.0478(2)	0.4680(6)	0.031(1)	C(41)	0.592(1)	0.4138(5)	0.292(1)	0.085(3)
C(3)	0.8665(6)	−0.1517(3)	0.4962(6)	0.040(2)	C(42)	0.4883(9)	0.4451(4)	0.2935(8)	0.062(2)
C(4)	0.6529(6)	0.1829(3)	0.4784(6)	0.039(2)	C(43)	0.3841(8)	0.5320(4)	0.3381(8)	0.055(2)
C(5)	0.5730(6)	0.1698(3)	0.5334(6)	0.040(2)					

[a] $U_{eq} = {}^1/_3\sum_i\sum_j U_{ij}a_i^*a_j^*\mathbf{a}_i\mathbf{a}_j$.

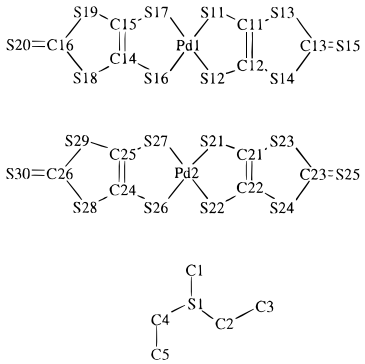

Figure 5. Atomic numbering scheme for (SMeEt$_2$)[Pd(dmit)$_2$]$_2$ (**7**).

were refined anisotropically in the space group *C*2/*m*. The final *R* values were $R = 0.047$ and $R_w = 0.049$.

(BTP)[Ni(dmit)$_2$]$_3$ (5). A black bar-shaped crystal of dimensions 0.63 × 0.15 x 0.08 mm^3 was used. Cell parameters were obtained by least-squares refinements on the basis of the setting angles of 22 reflections. Intensity data (8997 unique reflections with $h = -13$ to 13, $k = -27$ to 27, $l = 0-13$) were collected by the ω/θ scan technique in the θ range 1.5−23°. Reflections (4965) with $I > 3\sigma(I)$ were used in the calculations. All atoms except those belonging to phenyl groups (including H atoms) were refined anisotropically in the space group $P\bar{1}$. The final *R* values were $R = 0.049$ and $R_w = 0.051$.

(SMe$_3$)[Ni(dmit)$_2$]$_2$ (6). A plate-shaped crystal of dimensions 0.24 × 0.30 × 0.9 mm^3 was used. Intensity data (5502 unique reflections with $h = 0-9$, $k = -13$ to 13, $l = -21$ to 21) were collected by the $\omega/2\theta$ scan technique in the θ range 1.5−20°. Reflections (3147) with $I > 3\sigma(I)$ were used in the calculations. All non-hydrogen atoms were refined anisotropically in the space group $P\bar{1}$. The final *R* values were $R = 0.075$ and $R_w = 0.084$.

(SMeEt$_2$)[Pd(dmit)$_2$]$_2$ (7). A plate-shaped crystal of dimensions 0.40 × 0.30 × 0.05 mm^3 was used. Cell parameters were obtained by least-squares refinements on the basis of the setting angles of 15 reflections. Intensity data (4304 unique reflections with $h = -8$ to 8, $k = -38$ to 38, $l = 0-6$) were collected by the ω/θ scan technique in the θ range 1.5−22.5°. Reflections (3049) with $I > 3\sigma(I)$ were used in the calculations. All non-hydrogen atoms were refined anisotropically in the space group $P\bar{1}$. The final *R* values were $R = 0.074$ and $R_w = 0.093$.

Conductivity Measurements. Ambient pressure, room temperature compacted powder conductivity was measured on compressed pellets by using a Hewlett-Packard Model 4263A LCR meter. Temperature dependent (300−4 K) single-crystal conductivity measurements were carried out following the standard four-probe technique. Electrical contacts were obtained by gluing four gold wires to the crystal with Emetron M8001 gold paint. The sample mounted on a Motorola printed circuit was placed in an Oxford Instruments Model CF 200 continuous flow cryostat. Monitoring of the temperature variations and temperature resistance data acquisition was achieved by using an Oxford Instruments Model DTC2 PID temperature controller and the above-cited Hewlett-Packard device, both driven by a PC with homemade software.

Band Structure Calculations. The tight-binding band structure calculations are based upon the effective one-electron Hamiltonian of the extended Hückel method.[45] The off-diagonal matrix elements of the Hamiltonian were calculated according to the modified Wolfsberg−

(45) Hoffmann, R. *J. Chem. Phys.* **1963**, *39*, 1397. Whangbo, M.-H.; Hoffmann, R. *J. Am. Chem. Soc*. **1978**, *100*, 6093.

Table 7. Atomic Parameters for $(SMe_3)[Ni(dmit)_2]_2$ (**6**)

atom	*x*/*a*	*y*/*b*	*z*/*c*	U_{eq}[a] (Å^2)
Ni(1)	0.4325(1)	0.22192(7)	0.57267(5)	0.0268
S(1)	0.4007(2)	0.3842(1)	0.4857(1)	0.0338
S(2)	0.3408(2)	0.1212(1)	0.4994(1)	0.0337
S(3)	0.2760(2)	0.4366(1)	0.3235(1)	0.0347
S(4)	0.2197(2)	0.1922(1)	0.3369(1)	0.0346
S(5)	0.1515(3)	0.3647(2)	0.1894(1)	0.0509
S(6)	0.4692(2)	0.0571(1)	0.6583(1)	0.0349
S(7)	0.5086(2)	0.3251(1)	0.6492(1)	0.0311
S(8)	0.5853(2)	0.0049(2)	0.8224(1)	0.0385
S(9)	0.6186(3)	0.2517(2)	0.8144(1)	0.0419
S(10)	0.6915(3)	0.0770(2)	0.9614(1)	0.0506
C(1)	0.3257(8)	0.3408(5)	0.4107(4)	0.0246
C(2)	0.2949(8)	0.2242(5)	0.4178(4)	0.0182
C(3)	0.2137(9)	0.3323(6)	0.2794(4)	0.0347
C(4)	0.5375(8)	0.1018(6)	0.7344(4)	0.0255
C(5)	0.5531(8)	0.2196(6)	0.7301(4)	0.0283
C(6)	0.6355(9)	0.1085(6)	0.8707(4)	0.0354
Ni(1)	0.8449(1)	0.25935(6)	0.47698(5)	0.0255
S(11)	0.8195(2)	0.4249(1)	0.3930(1)	0.0328
S(12)	0.7665(2)	0.1604(1)	0.3987(1)	0.0300
S(13)	0.7063(3)	0.4838(1)	0.2285(1)	0.0357
S(14)	0.6571(3)	0.2410(2)	0.2337(1)	0.0382
S(15)	0.5960(4)	0.4213(2)	0.0878(1)	0.0554
S(16)	0.8752(2)	0.0933(1)	0.5608(1)	0.0331
S(17)	0.9321(2)	0.3565(1)	0.5544(1)	0.0339
S(18)	1.0093(2)	0.0306(1)	0.7210(1)	0.0340
S(19)	1.0620(2)	0.2734(2)	0.7155(1)	0.0352
S(20)	1.1487(3)	0.0864(2)	0.8566(1)	0.0446
C(11)	0.7516(8)	0.3838(5)	0.3152(4)	0.0236
C(12)	0.7265(8)	0.2695(5)	0.3177(4)	0.0210
C(13)	0.653(1)	0.3843(6)	0.1791(4)	0.0379
C(14)	0.9529(8)	0.1324(5)	0.6364(4)	0.021
C(15)	0.9779(8)	0.2474(5)	0.6333(4)	0.0226
C(16)	0.10758(9)	0.1295(6)	0.7693(4)	0.0323
S(21)	0.0587(4)	0.3257(2)	1.0191(1)	0.0527
C(210)	−0.045(2)	0.3495(8)	0.9307(6)	0.0764
C(211)	−0.011(1)	0.1905(7)	1.0701(5)	0.0551
C(212)	0.273(1)	0.2762(9)	0.9942(6)	0.0685

[a] $U_{eq} = {}^1/_3\sum_i\sum_j U_{ij}a_i^*a_j^*\mathbf{a}_i\mathbf{a}_j$.

Hemholz formula.[46] All valence electrons were explicitly taken into account in the calculations. The basis set consisted of Slater type orbitals of double-ζ quality for Pd 4d and single-ζ quality for Pd 5s and 5p, S 3s and 3p, and C 2s and 2p. The exponents, contraction coefficients of the double-ζ orbitals, and atomic parameters used for the calculations were taken from previous work.[47]

Results and Discussion

Synthesis and Crystal Structure of $[ML_2]^{n-}$ Complexes (L = dmit^{2-}, dddt^{2-}, and dtdt^{2-}; *n* = 2 or 1). Both the dddt^{2-} and dtdt^{2-} ligands have been obtained as their potassium salts by hydrolysis of the appropriate thione, $C_5H_4S_5$ and $C_5H_4S_6$, respectively (Scheme 1). It is interesting to note that both of these thiones are obtained from dmit-based compounds, *e.g.*, $dmitNa_2$ or $(NR_4)_2[Zn(dmit)_2]$, respectively, by ring closure with dibromoethane or dichloromethyl sulfide, respectively.

The $(cation)_n[ML_2]$ complexes (L = dmit^{2-}, dddt^{2-}, and dtdt^{2-}) are obtained by complexation of the ligand L with an appropriate metal salt and precipitation with a salt of the appropriate cation. Whereas in the case of the dmit^{2-} ligand the expected divalent $[cation)_2[M(dmit)_2]$ complexes (cation = NR_4^+, PPN^+, BTP^+, $(SMe_yEt_{3-y})^+$] are readily obtained, in the case of both the dddt^{2-} and dtdt^{2-} ligands, the monovalent $(NR_4)[ML_2]$ complexes are directly obtained, even under a nonoxidating atmosphere. Facile oxidation of the (NR_4)-$[M(dddt)_2]$ complexes affording the neutral $[M(dddt)_2]^0$ species is observed, whereas only one neutral dmit-based complex, namely, $[Ni(dmit)_2]^0$, has been obtained as a minority product in the preparation of the charge transfer salt (TTF)$[Ni(dmit)_2]_2$.[26b] Oxidation of the $(NR_4)[M(dtdt)_2]$ complexes, affording the neutral $[M(dtdt)_2]^0$ species, is also possible (*vide infra*).

Table 8. Atomic Parameters for $(SMeEt_2)[Pd(dmit)_2]_2$ (**7**)

atom	*x*/*a*	*y*/*b*	*z*/*c*	U_{eq}[a] (Å^2)
Pd(1)	0.1881(1)	0.48158(3)	1.0179(2)	0.0295
Pd(2)	0.1852(1)	0.01891(3)	1.0217(2)	0.0289
S(1)	0.451(1)	0.2523(2)	0.768(1)	0.1008
S(11)	0.0366(5)	0.4342(1)	0.7698(6)	0.0354
S(12)	0.1982(5)	0.44734(9)	1.3231(6)	0.0349
S(13)	−0.0655(6)	0.3591(1)	0.8591(7)	0.0441
S(14)	0.0798(6)	0.3702(1)	1.3493(6)	0.0415
S(15)	−0.0900(8)	0.2983(1)	1.1519(9)	0.0620
S(16)	0.3559(5)	0.5263(1)	1.2695(6)	0.0369
S(17)	0.1962(5)	0.51507(9)	0.7176(6)	0.0358
S(18)	0.5048(6)	0.5979(1)	1.1966(6)	0.0422
S(19)	0.3647(6)	0.5879(1)	0.7064(6)	0.0415
S(20)	0.5609(7)	0.6565(1)	0.9138(9)	0.0539
S(21)	0.1965(5)	−0.01456(9)	0.7111(6)	0.0341
S(22)	0.3593(5)	−0.0258(1)	1.2606(6)	0.0354
S(23)	0.3714(6)	−0.0872(1)	0.6774(6)	0.0395
S(24)	0.5155(5)	−0.0972(1)	1.1673(6)	0.0391
S(25)	0.5766(7)	−0.1561(1)	0.8650(8)	0.0544
S(26)	0.1901(5)	0.0533(1)	1.3354(6)	0.0357
S(27)	0.0284(5)	0.0658(1)	0.7860(6)	0.0357
S(28)	0.0602(6)	0.1306(1)	1.3801(7)	0.0434
S(29)	−0.0849(6)	0.1413(1)	0.8919(7)	0.0475
S(30)	−0.1161(8)	0.2025(1)	1.201(1)	0.0684
C(1)	0.402(5)	0.222(2)	0.597(5)	0.0692
C(2)	0.475(4)	0.283(1)	0.563(5)	0.1160
C(3)	0.648(5)	0.270(1)	0.502(6)	0.1464
C(4)	0.213(4)	0.2626(8)	0.731(4)	0.1011
C(5)	0.162(5)	0.236(1)	0.872(6)	0.1491
C(11)	0.028(2)	0.4022(4)	0.954(2)	0.0206
C(12)	0.099(2)	0.4071(3)	1.192(2)	0.0259
C(13)	−0.028(2)	0.3400(4)	1.123(3)	0.0463
C(14)	0.387(2)	0.5577(4)	1.095(2)	0.0282
C(15)	0.316(2)	0.5526(4)	0.859(2)	0.0332
C(16)	0.480(2)	0.6169(4)	0.941(3)	0.0420
C(21)	0.325(2)	−0.0519(4)	0.844(2)	0.0350
C(22)	0.390(2)	−0.0570(4)	1.073(2)	0.0319
C(23)	0.487(2)	−0.1163(4)	0.905(2)	0.0355
C(24)	0.086(2)	0.0934(4)	1.215(2)	0.0249
C(25)	0.017(2)	0.0984(4)	0.983(2)	0.0300
C(26)	−0.054(2)	0.1602(5)	1.157(3)	0.0456

[a] $U_{eq} = {}^1/_3\sum_i\sum_j U_{ij}a_i^*a_j^*\mathbf{a}_i\mathbf{a}_j$.

Scheme 1

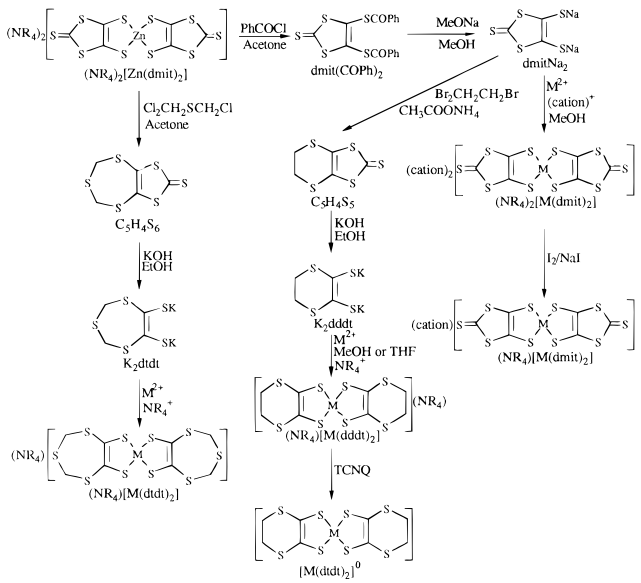

(46) Ammeter, J.; Bürgi, H.-B.; Thibeault , J.; Hoffmann, R. *J. Am. Chem. Soc*. **1978**, *100*, 3686.
(47) Canadell E.; Rachidi E.-I.; Ravy S.; Pouget J.-P.; Brossard L.; Legros J.-P. *J. Phys. Fr.* **1989**, *50*, 2967.

Table 9. Selected Bond Distances and Angles (deg) for $(NBu_4)[Pt(dtdt)_2]$ (**1**)

Pt(1)−S(1)	2.261(3)	S(3)−C(1)	1.75(1)	S(6)−C(6)	1.73(1)	S(10)−C(7)	1.79(1)
Pt(1)−S(2)	2.259(3)	S(3)−C(3)	1.81(1)	S(7)−C(5)	1.72(1)	S(10)−C(8)	1.78(1)
Pt(1)−S(6)	2.268(3)	S(4)−C(2)	1.76(1)	S(8)−C(6)	1.75(1)	C(1)−C(2)	1.38(1)
Pt(1)−S(7)	2.255(3)	S(4)−C(4)	1.80(1)	S(8)−C(8)	1.81(1)	C(5)−C(6)	1.36(1)
S(1)−C(1)	1.71(1)	S(5)−C(3)	1.78(1)	S(9)−C(5)	1.77(1)		
S(2)−C(2)	1.71(1)	S(5)−C(4)	1.79(1)	S(9)−C(7)	1.80(1)		

S(1)−Pt(1)−S(2)	88.5(1)	Pt(1)−S(6)−C(6)	104.0(4)	S(3)−C(3)−S(5)	117.3(6)
S(1)−Pt(1)−S(6)	175.2(1)	Pt(1)−S(7)−C(5)	103.8(4)	S(4)−C(4)−S(5)	118.0(6)
S(2)−Pt(1)−S(6)	92.07(9)	C(6)−S(8)−C(8)	103.8(5)	S(7)−C(5)−S(9)	113.3(6)
S(1)−Pt(1)−S(7)	90.7(1)	C(5)−S(9)−C(7)	101.3(6)	S(7)−C(5)−C(6)	122.4(8)
S(2)−Pt(1)−S(7)	179.2(1)	C(7)−S(10)−C(8)	101.8(5)	S(9)−C(5)−C(6)	124.2(8)
S(6)−Pt(1)−S(7)	88.7(1)	S(1)−C(1)−S(3)	114.9(6)	S(6)−C(6)−S(8)	115.7(6)
Pt(1)−S(1)−C(1)	104.5(4)	S(1)−C(1)−C(2)	121.3(8)	S(6)−C(6)−C(5)	120.6(8)
Pt(1)−S(2)−C(2)	104.6(3)	S(3)−C(1)−C(2)	123.8(8)	S(8)−C(6)−C(5)	123.6(8)
C(1)−S(3)−C(3)	103.5(4)	S(2)−C(2)−S(4)	115.1(6)	S(9)−C(7)−S(10)	117.7(7)
C(2)−S(4)−C(4)	102.8(5)	S(2)−C(2)−C(1)	121.1(8)	S(8)−C(8)−S(10)	117.0(6)
C(3)−S(5)−C(4)	100.1(5)	S(4)−C(2)−C(1)	123.8(8)		

Table 10. Selected Bond Distances and Angles (deg) for (PPN)[Ni(dmit)2]·$(CH_3)_2CO$ (**2**)

Ni(1)−S(1)	2.165(2)	Ni(1)−S(2)	2.160(2)	Ni(1)−S(6)	2.161(2)	Ni(1)−S(7)	2.167(2)
S(1)−C(1)	1.711(8)	S(2)−C(2)	1.714(8)	S(3)−C(1)	1.738(8)	S(3)−C(3)	1.746(9)
S(4)−C(2)	1.742(8)	S(4)−C(3)	1.723(8)	S(5)−C(3)	1.636(8)	S(6)−C(4)	1.722(8)
S(7)−C(5)	1.699(8)	S(8)−C(4)	1.740(8)	S(8)−C(6)	1.736(9)	S(9)−C(5)	1.740(8)
S(9)−C(6)	1.72(1)	S(10)−C(6)	1.640(9)	N(1)−P(1)	1.567(6)	N(1)−P(2)	1.594(6)
P(1)−C(7)	1.799(7)	P(1)−C(13)	1.795(8)	P(1)−C(19)	1.792(7)	P(2)−C(25)	1.796(7)
P(2)−C(31)	1.803(8)	P(2)−C(37)	1.789(8)	C(1)−C(2)	1.36(1)	C(4)−C(5)	1.37(1)

S(1)−Ni(1)−S(2)	92.83(8)	S(6)−Ni(1)−S(7)	93.11(9)	Ni(1)−S(1)−C(1)	102.5(3)
Ni(1)−S(2)−C(2)	103.3(3)	C(1)−S(3)−C(3)	97.4(4)	C(2)−S(4)−C(3)	97.7(4)
Ni(1)−S(6)−C(4)	102.3(3)	Ni(1)−S(7)−C(5)	102.2(3)	C(4)−S(8)−C(6)	97.0(4)
C(5)−S(9)−C(6)	98.4(4)	P(1)−N(1)−P(2)	137.9(4)	N(1)−P(1)−C(7)	114.2(3)
N(1)−P(1)−C(13)	112.5(3)	C(7)−P(1)−C(13)	108.9(3)	N(1)−P(1)−C(19)	107.1(3)
C(7)−P(1)−C(19)	106.5(3)	C(13)−P(1)−C(19)	107.3(3)	N(1)−P(2)−C(25)	112.8(3)
N(1)−P(2)−C(31)	112.8(3)	C(25)−P(2)−C(31)	108.4(3)	N(1)−P(2)−C(37)	107.8(3)
C(25)−P(2)−C(37)	107.2(3)	C(31)−P(2)−C(37)	107.7(3)	S(1)−C(1)−C(2)	120.8(6)
S(3)−C(1)−C(2)	116.1(6)	S(2)−C(2)−C(1)	121.5(6)	S(4)−C(2)−C(1)	116.0(6)
S(3)−C(3)−S(4)	112.8(5)	S(3)−C(3)−S(5)	123.3(5)	S(4)−C(3)−S(5)	124.0(5)
S(6)−C(4)−C(5)	120.5(6)	S(8)−C(4)−C(5)	116.9(6)	S(7)−C(5)−C(4)	122.0(6)
S(9)−C(5)−C(4)	114.7(6)	S(8)−C(6)−S(9)	113.0(5)	S(8)−C(6)−S(10)	123.4(6)
S(9)−C(6)−S(10)	123.6(6)				

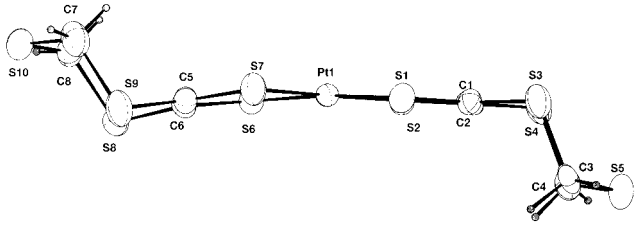

Figure 6. Side view of the $[Pt(dtdt)_2]^-$ anion in $(NBu_4)[Pd(dtdt)_2]$ (**1**).

All prepared $[ML_2]^{n-}$ complexes (L = $dmit^{2-}$, $dddt^{2-}$, and $dtdt^{2-}$; n = 2, 1, or 0) have been characterized by elemental analysis and infrared spectroscopy. Further characterization is provided by the determination of the crystal structures of $(NBu_4)[Pt(dtdt)_2]$ (**1**), (PPN)[Ni(dmit)$_2$]·$(CH_3)_2CO$ (**2**), and $(SMeEt_2)[Ni(dmit)_2]$ (**3**).

$(NBu_4)[Pt(dtdt)_2]$ (1). Selected bond lengths and angles are listed in Table 9. A side view of the $[Pt(dtdt)_2]^-$ anion is shown in Figure 6. The anion adopts a chair conformation: the central part is almost planar (largest deviation = ±0.27 Å, dihedral angle between the two PtC_2S_4 moieties = 9.25°), and the two external C_2S planes lie above and below this plane at a distance of ≈1.6 Å. This structure is very similar to that of the analogue $(NBu_4)[Ni(dtdt)_2]$ complex.[29] The averaged Pt−S distances in **1** (2.261 Å) are comparable to those found for other monovalent 1,2-dithiolate platinum complexes, such as $(NBu_4)[Pt(dmit)_2]$ (2.28 Å)[48] or $(NEt_4)[Pt(dddt)_2]$ (2.27 Å).[49] With the exception of the M−S distances, the intramolecular distances in the $[Pt(dtdt)_2]^-$ anion are almost similar to those found in (NBu_4)-$[Ni(dtdt)_2]$.[29]

(PPN)[Ni(dmit)$_2$]·$(CH_3)_2CO$ (2). Selected bond lengths and angles are listed in Table 10. The averaged intramolecular distances and angles within the $[Ni(dmit)_2]$ unit are in agreement with those found for $(NBu_4)[Ni(dmit)_2]$.[48,50] The unit cell contains two $[Ni(dmit)_2]^-$ units, two PPN^+ cations and two acetone molecules. The structure consists of layers of [Ni-$(dmit)_2$] units lying side by side (Figure 7a). These layers, separated by sheets of cations and solvent molecules, are built of infinite chains of $Ni(dmit)_2$ entities connected to each other by short S···S contacts and running along [100] (Figure 7b). No short S···S contacts are observed between the chains. The distances within the PPN^+ cation are similar to those found in other PPN^+ salts.[51] The PPN^+ cation adopts a bent structure [angle P−N−P = 137.9(4)°], which is the usual geometry for the PPN^+ cation.[51]

$(SMeEt_2)[Ni(dmit)_2]$ (3). Selected bond lengths and angles are listed in Table 11. The averaged intramolecular distances and angles within the $[Ni(dmit)_2]$ unit are in agreement with those found for (PPN)[Ni(dmit)$_2$]·$(CH_3)_2CO$ (**2**) and (NBu_4)-$[Ni(dmit)_2]$.[48,50] The projection of the structure onto the *bc* plane is shown in Figure 8a. The structure consists of $[Ni(dmit)_2]$

(48) (a) Mentzafos, D.; Hountas, A. *Acta Crystallogr.* **1988**, *C44*, 1550. (b) Baumer, V. N.; Starodub, V. A.; Tarasova, G. E. *Sov. Phys. Crystallogr.* **1989**, *34*, 59.

(49) Welch, J. H.; Bereman, R. D.; Singh, P. *Inorg. Chim. Acta* **1989**, *163*, 93−98.

(50) Lindqvist, O.; Andersen, L.; Sieler, J .; Steimecke, G; Hoyer, E. *Acta Chem. Scand.* **1982**, *A36*, 855.

(51) Wilson, R. D.; Bau, R. *J. Am. Chem. Soc.* **1974**, *96*, 7601

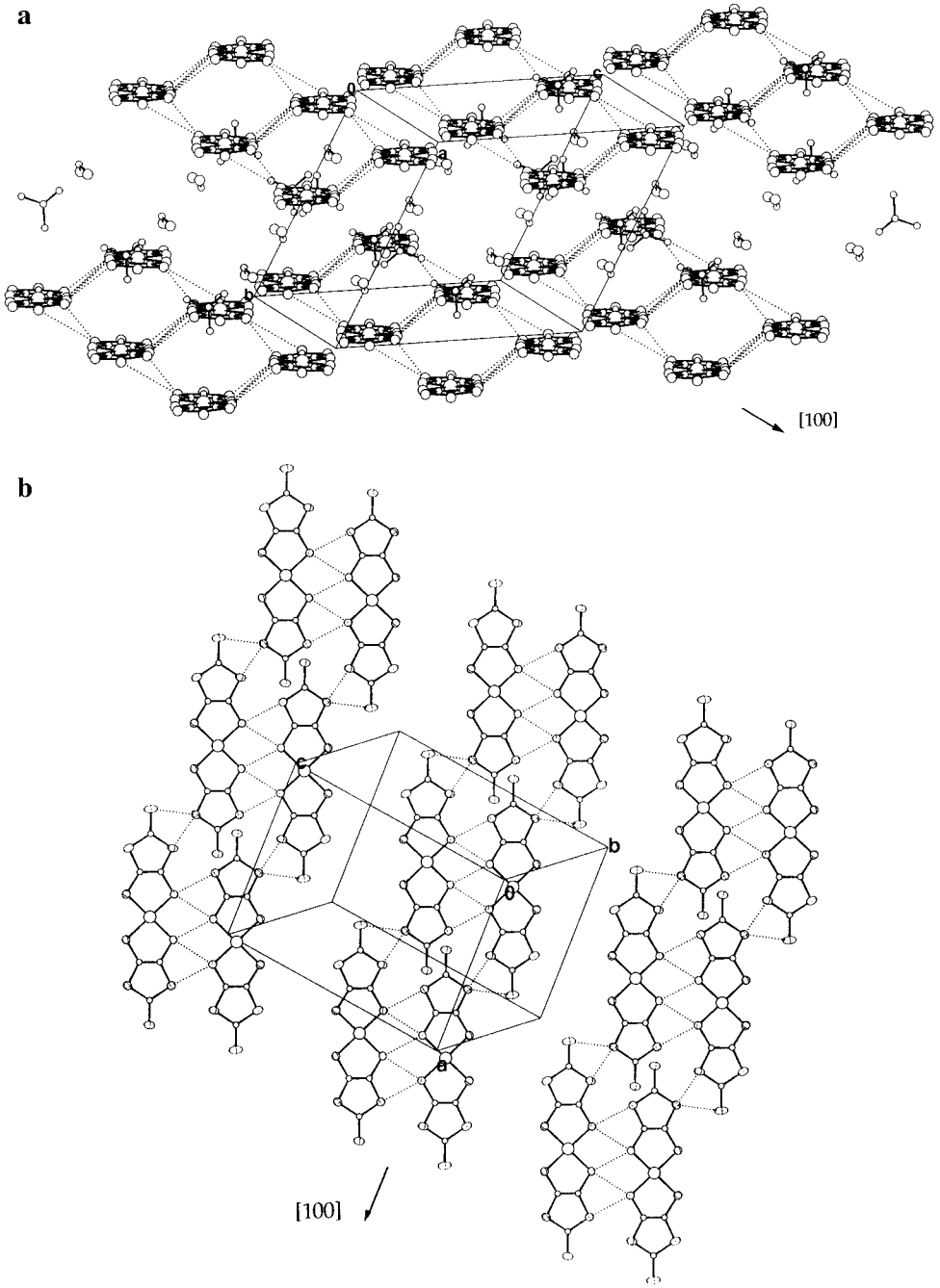

Figure 7. (PPN)[Ni(dmit)$_2$]·(CH$_3$)$_2$CO (**2**): (a) projection along the long axis of the Ni(dmit)$_2$ units [for clarity, only the Ni(dmit)$_2$, C−CO−C, and P−N−P moieties are represented; dotted lines represent the S···S distances shorter than the sum of the van der Waals radii (3.7 Å)]; (b) projection perpendicular to the plane of the Ni(dmit)$_2$ units.

Table 11. Selected Bond Distances and Angles (deg) for (SMeEt$_2$)[Ni(dmit)$_2$] (**3**)

Ni(1)−S(1)	2.173(2)	S(2)−C(2)	1.715(6)	S(5)−C(3)	1.643(7)	S(9)−C(5)	1.744(6)
Ni(1)−S(2)	2.157(2)	S(3)−C(1)	1.739(7)	S(6)−C(4)	1.707(7)	S(9)−C(6)	1.740(7)
Ni(1)−S(6)	2.153(2)	S(3)−C(3)	1.734(7)	S(7)−C(5)	1.709(6)	S(10)−C(6)	1.631(7)
Ni(1)−S(7)	2.171(2)	S(4)−C(2)	1.741(6)	S(8)−C(4)	1.734(7)	C(1)−C(2)	1.356(8)
S(1)−C(1)	1.715(7)	S(4)−C(3)	1.721(7)	S(8)−C(6)	1.721(7)	C(4)−C(5)	1.363(8)

Ni(1)−S(1)−C(1)	101.9(2)	S(3)−C(3)−S(4)	112.294)	S(8)−C(6)−S(9)	112.1(4)
Ni(1)−S(2)−C(2)	101.9(2)	S(3)−C(3)−S(5)	124.1(4)	S(8)−C(6)−S(10)	123.9(4)
Ni(1)−S(6)−C(4)	102.9(2)	S(4)−C(2)−C(1)	116.3(5)	S(9)−C(5)−C(4)	115.2(5)
Ni(1)−S(7)−C(5)	102.2(2)	S(4)−C(3)−S(5)	123.6(4)	S(9)−C(6)−S(10)	124.0(4)
S(1)−Ni(1)−S(2)	93.24(7)	S(6)−C(4)−C(5)	120.9(5)	C(1)−S(3)−C(3)	98.3(3)
S(1)−C(1)−C(2)	121.0(5)	S(6)−Ni(1)−S(7)	92.67(7)	C(2)−S(4)−C(3)	98.0(3)
S(2)−C(2)−C(1)	122.0(5)	S(7)−C(5)−C(4)	121.3(5)	C(4)−S(8)−C(6)	98.4(3)
S(3)−C(1)−C(2)	115.2(5)	S(8)−C(4)−C(5)	116.2(5)	C(5)−S(9)−C(6)	98.1(3)

units parallel to the *bc* plane and connected to each other through short S···S (<3.70 Å) contacts, via either the cation (SMeEt$_2$)$^+$ or their own sulfur atoms. The Ni(dmit)$_2$ entities form zig-zag stacks along the [100] direction (Figure 8b).

Compared Electrochemical Behavior of the [ML$_2$]$^{n-}$ Complexes Studied (L = dmit^{2-}, dtdt^{2-}, and dddt^{2-}). The electrochemical behavior of (NR$_4$)[Ni(dmit)$_2$] complexes has been previously studied in detail.[38] From these studies, the

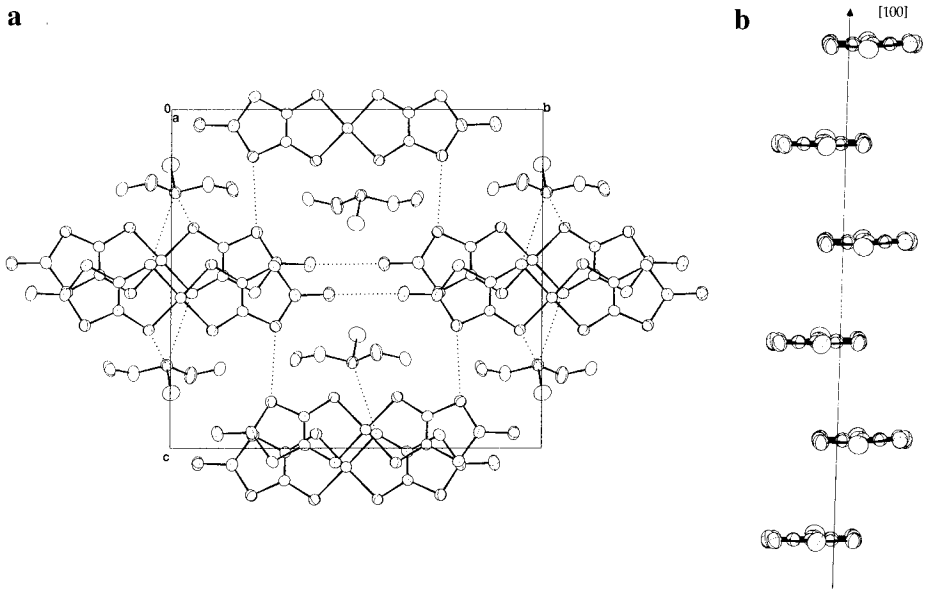

Figure 8. (a) Projection of $(SMeEt_2)[Ni(dmit)_2]$ (**3**) onto the *bc* plane. (b) Side view of the along the [100] direction.

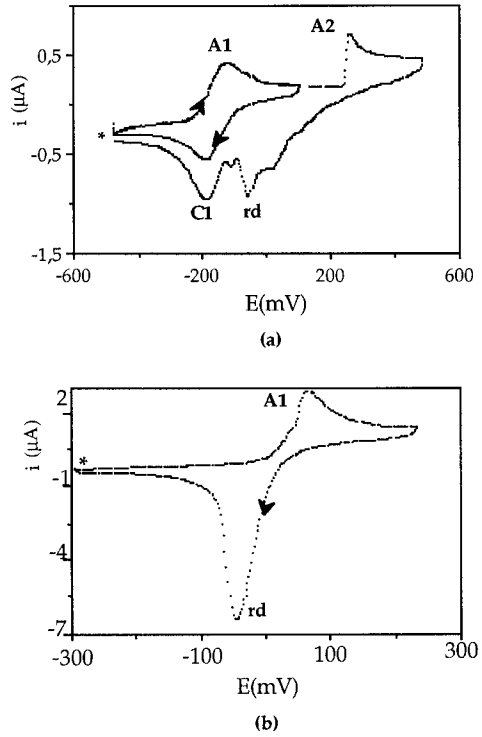

Figure 9. Cyclic voltammograms of (a) $(SMe_3)[Ni(dmit)_2]$ (10^{-3} M) and (b) $(SMe_3)[Pd(dmit)_2]$ (10^{-3} M), in $CH_3CN/(SMe_3)BF_4$ (10^{-1} M) at a Pt electrode (1 mm) with a scan rate of 0.1 V s^{-1} [potential in volts *vs* Ag/AgCl (* starting potential)].

following mechanism for the formation of the derived (NR_4)-$[Ni(dmit)_2]_z$ NIOS complexes has been proposed:

$$[Ni(dmit)_2]^{2-} \leftrightarrows [Ni(dmit)_2]^{-} \quad (1)$$

$$[Ni(dmit)_2]^{-} \rightleftarrows [Ni(dmit)_2]^{0} \quad (2)$$

$$n[Ni(dmit)_2]^{-} + m[Ni(dmit)_2]^{0} \rightarrow \{[Ni(dmit)_2]^{x-}\}_{n+m} \quad (3)$$

where $x = 1/z = n/(n + m)$. (1) The first one-electron transfer, which appears quasi-reversible at any potential scan rate, corresponds to the $[Ni(dmit)_2]^{2-}/[Ni(dmit)_2]^{-}$ couple. (2) The second electron transfer, which appears quasi-reversible only at fast potential scan rates, generates the neutral species $[Ni(dmit)_2]^0$. (3) The NIOS radical anion $\{[Ni(dmit)_2]^{x-}\}_{n+m}$ is formed by a chemical reaction, in the diffusion layer, between $[Ni(dmit)_2]^{-}$ and $[Ni(dmit)_2]^0$ species. This compound, being insoluble, is deposited on the anode.

In the present work, the (cation)$[M(dmit)_2]$ complexes studied with M = Ni, Pt and cation = PPN^+, BTP^+, and $(SMe_yEt_{3-y})^+$ and the (cation)$[Pd(dmit)_2]$ complexes with cation = PPN^+, BTP^+ exhibit similar electrochemical behavior (Figure 9a, and Figure S1 and Table S26 in the supplementary material), and the same mechanism can be applied to the formation of their derived NIOS compounds. In the cyclic voltammogram of the $(SMe_yEt_{3-y})_2[Pd(dmit)_2]$ complexes, only one, instead of two, redox wave is observed (Figure 9b and Figure S1 and Table S26 in the supplementary material), indicating that reactions 1−3 take place simultaneously at the same potential. This explains why the monovalent $(SMe_yEt_{3-y})[Pd(dmit)_2]$ complexes could not be obtained by iodine oxidation of the corresponding divalent $(SMe_yEt_{3-y})_2[Pd(dmit)_2]$ complexes (see the Experimental Section).

The electrochemical behavior of $(NR_4)[M(dddt)_2]$ complexes (M = Ni, Pt) has also been previously described and discussed[39] and is quite different from that of the (cation)$[M(dmit)_2]$ complexes. From these studies, the following mechanism has been proposed:

$$[M(dddt)_2]^{2-} \leftrightarrows [M(dddt)_2]^{-} \quad (1')$$

$$[M(dddt)_2]^{-} \rightleftarrows [M(dddt)_2]^{0} \quad (2')$$

$$n[M(dddt)_2]^{-} + m[M(dddt)_2]^{0} \rightarrow \{[M(dddt)_2]^{x-}\}_{n+m} \quad (3')$$

$$[M(dddt)_2]^{0} \leftrightarrows [M(dddt)_2]^{+} \quad (4')$$

$$p[M(dddt)_2]^{0} + q[M(dddt)_2]^{+} \rightarrow \{[M(dddt)_2]^{x+}\}_{p+q} \quad (5')$$

where $x = q/(p + q)$.

$$[Ni(dddt)_2]^{+} - (\text{oxidation}-\text{decomposition}) \rightarrow \text{organic radicals} \quad (6')$$

(1′−3′) The first two oxidation waves observed, which are quasi-reversible even at low scan rate, correspond to the $[M(dddt)_2]^{2-}/[M(dddt)_2]^{-}$ and $[M(dddt)_2]^{-}/[M(dddt)_2]^{0}$ couples. In the present case, reaction 3′, which could have been expected

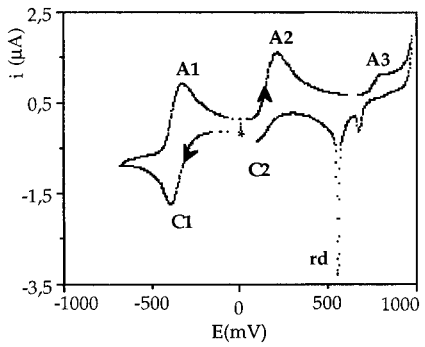

Figure 10. Cyclic voltammogram of $(NEt_4)[Pd(dddt)_2]$ (10^{-3} M) in acetone/$(NEt_4)BF_4$ (10^{-1} M) at a Pt electrode (1 mm) with a scan rate of 0.1 V s^{-1} [potential in volts *vs* Ag/AgCl (* starting potential)].

between the $[M(dddt)_2]^-$ and $[M(dddt)_2]^0$ species, does not seem to take place. (4′) A third electron transfer, which appears quasi-reversible only at fast potential scan rates, generates the $[M(dddt)_2]^+$ cation. (5′) The formation of the $\{[M(dddt)_2]^{x+}\}_{p+q}$ radical cation, from which several examples of salts have been reported,[52−55] results from the reaction between the $[M(dddt)_2]^0$ and $[M(dddt)_2]^+$ species. (6′) In the case of the nickel compounds, oxidation−decomposition processes make the mechanism more complicated and explain the irreversibility of the third wave.[39]

The previous studies on nickel and platinum $(NR_4)[M(dddt)_2]$ complexes[39] have been extended to the palladium analogue complex. The behavior of $(NEt_4)[Pd(dddt)_2]$ (Figure 10 and Figure S1 and Table S26 in the supplementary material) is quite similar to that of the platinum analogue complex and confirms the proposed mechanism. Thus, the $[M(dddt)_2]$ complexes may be readily used for the preparation of NIOS radical cation salts.[52−55] Moreover, the $[M(dddt)_2]$ complexes may also be used as donor molecules in the preparation of $[M(dddt)_2][M'(dmit)_2]_x$ compounds (*vide infra*). By contrast, as reaction 3′ does not seem to take place, the preparation of (cation)-$[M(dddt)_2]_z$ NIOS radical anion salts should not be possible.

In the case of the $(NR_4)[M(dtdt)_2]$ complexes, the cyclic voltammetry data were deceiving at first sight. The cyclic voltammogram of these complexes in acetonitrile (Figure 11 and Figure S1 and Table S27 in the supplementary material) looks quite similar to those of the $(NR_4)[M(dmit)_2]$ complexes[38] and consists of two waves, a first quasi-reversible one corresponding to the $[M(dtdt)_2]^{2-}/[M(dtdt)_2]^-$ couple and a second one exhibiting the typical features associated with the deposition of a conductive species on the anode:[38] a fast increase in the current of the anodic peak, the presence of an intense backward peak characteristic of a redissolution process, the observation of a black deposit on the anode, and an increase in the peak's intensity on a subsequent potential scan to more anodic potentials. When the potential scan rate is increased, the intensity of the redissolution peak decreases. At 800 V s^{-1} for the nickel compound and 300 V s^{-1} for the platinum compound, the electron transfer becomes reversible and generates the neutral $[M(dtdt)_2]^0$ species (Figure 11b). From these results, it could be inferred that the $\{[M(dtdt)_2]^{x-}\}_{n+m}$ radical anion could be generated by electrocrystallization.[29] Conversely, under stationary conditions (Figure 11c), the reversibility was established for both waves by standard tests (Nernstian shape, diffusion-controlled process, peak intensity),[56] and coulometry experiments show that one electron is accounted for both transfers. Finally, in benzonitrile the second wave is quasi-reversible, even at low scan rate, and no typical features that could be associated with the deposition of a conductive species are observed (Figure 11d).

Still, the typical features associated with the deposition of a conductive species on the anode observed in acetonitrile remain to be explained. Galvanostatic electrocrystallization of acetonitrile solutions of $(NR_4)[M(dtdt)_2]$ (M = Ni, Pt) yields shiny needle-shaped crystals.[31] These samples exhibit poor powder conductivities (10^{-7} and 10^{-3} S cm^{-1}, respectively), and the elemental analyses were compatible with the formulas for the corresponding neutral $[M(dtdt)_2]^0$ species.

In conclusion, oxidation of the $[M(dtdt)_2]^-$ complexes in acetonitrile as well as in benzonitrile, and at any potential scan rate, yields the neutral $[M(dtdt)_2]^0$ species instead of the $\{[M(dtdt)_2]^{x-}\}_{n+m}$ NIOS radical anion, and the reaction of type 3 between the monoanion and the neutral species, observed in the case of the $[M(dmit)_2]$ complexes, does not take place in the case of the $[M(dtdt)_2]$ complexes. Whereas $[M(dtdt)_2]^0$ is soluble in benzonitrile, it is insoluble in acetonitrile and is deposited on the anode. However, its conductivity is sufficiently high to not passivate the electrode.

$[M(dddt)_2][M'(dmit)_2]_x$ Compounds. As discussed earlier, the $[M(dddt)_2]$ complexes may be used for the preparation of NIOS radical cation salts, such as $[Ni(dddt)_2]_3X_2$ with X = BF_4^-,[52] HSO_4^-,[53] $AuBr_2^-$,[54] $[Pt(dddt)_2]_2X$ with X = IBr_2^-, ICl_2^-, $AuBr_2^-$,[55] and $[Pd(dddt)_2]_2X$ with X = $Ag_xBr_y^-$, $AuBr_2^-$, PF_6^-.[54] We have prepared bimetallic compounds $[M(dddt)_2][M'(dmit)_2]_x$ (M, M′ = Ni, Ni; Ni, Pd; Pt, Ni; Pt, Pd), in which $[M(dddt)_2]$ and $[M'(dmit)_2]$ play the roles of a donor cation and an acceptor anion, respectively (see the Experimental Section). Crystalline samples have been obtained in all cases, and their powder conductivity is rather modest (10^{-3}−10^{-5} S cm^{-1}). Their stoichiometry could not be inferred with certainty from just elemental analyses. In one case (M, M′ = Pt, Ni), the crystal quality allowed an X-ray structural study, from which a 1/2 stoichiometry has been determined.

Selected bond lengths and angles for $[Pt(dddt)_2][Ni(dmit)_2]_2$ (**4**) are listed in Table 12. No significant differences can be observed between the intramolecular distances in the $Pt(dddt)_2$ entity and the distances observed for the neutral $Pt(dddt)_2$ compound.[35] On the contrary, if most of the distances within the $Ni(dmit)_2$ unit are similar to those found for the $[Ni(dmit)_2]^{n-}$ complexes, the averaged Ni−S and S−C distances (2.134 and 1.67 Å, respectively) are even shorter than those observed for the neutral $Ni(dmit)_2$ compound (2.147 and 1.699 Å).[26b] This may indicate that the delocalization is very important in the central rings of the $Ni(dmit)_2$ unit, following the model proposed by Schrauzer.[57] The structure consists of stacks along [010] of $Ni(dmit)_2$ planar entities perpendicular to $Pt(dddt)_2$ entities, which are also planar with the exception of their terminal CH_2-CH_2 groups (Figure 12a). The $Ni(dmit)_2$ stacks are separated by layers of the $Pt(dddt)_2$ entities lying side by side. Short S···S contacts only exist between the $Ni(dmit)_2$ and $Pt(dddt)_2$ units but not within the $Ni(dmit)_2$ stacks, although the interplanar distance is 3.60 Å (Figure 12b). In spite of a promising stoichiometry, which could involve a partial oxidation state for either the $[Pt(dddt)_2]$ and/or the $[Ni(dmit)_2]$ components (unless the charge transfer is zero), this type of structural arrangement

(52) Yagubskii, E. B.; Kotov, A. I.; Buravov, L. I.; Khomenko, A. G.; Shklover, B. E.; Nahapetyan, S. S.; Struchkov, Yu. T.; Vetoshkina, L. V.; Ukhin, L. Yu. *Synth. Metals* **1990**, *35*, 271.
(53) Yagubskii, E. B.; Kotov, A. I.; Khomenko, A. G.; Buravov, L. I.; Schegolev, V. E.; Shibaeva, R. P. *Synth. Metals* **1991**, *46*, 255.
(54) Yagubskii, E. B.; Kushch, L. A.; Gritsenko, V. V.; Dyachenko, O. A.; Buravov, L. I.; Khomenko, A. G. *Synth. Metals* **1995**, 70, 1039.
(55) Yagubskii, E. B., Kotov, A. I.; Laukhina, E. E.; Ignatiev, A. A.; Khomenko, A. G.; Nahapetyan, S. S.; Shklover, B. E.; Struchkov, Yu. T.; Vetoshkina, L. V.; Ukhin, L. Yu. *Mater. Sci.* **1991**, *17*, 55.
(56) Bard, A.; Faulkner, L. R. *Electrochemical Methods*; J. Wiley & Sons: New York, 1980.
(57) Schrauzer, G. N. *Acc. Chem. Res.* **1969**, *2*, 72.

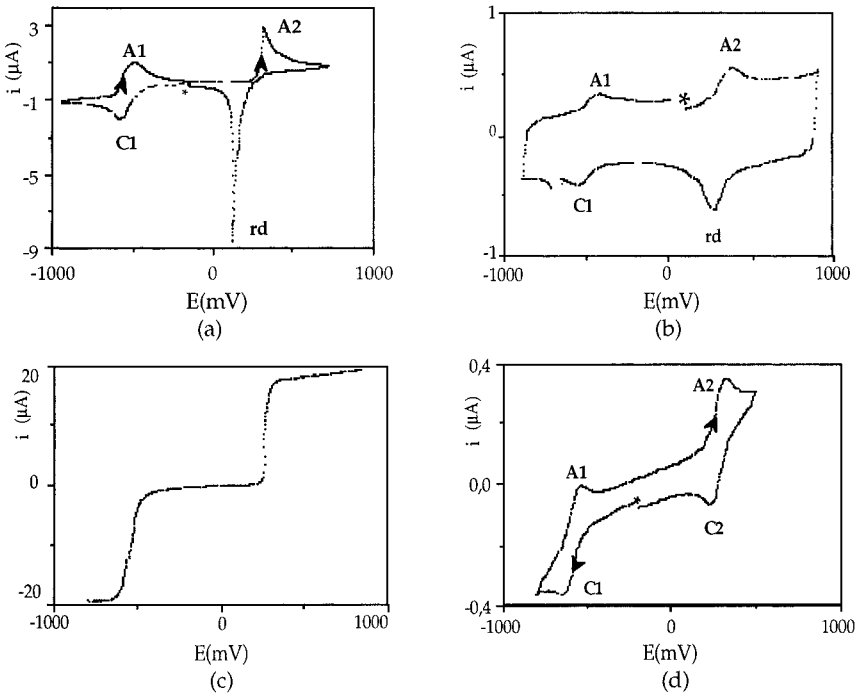

Figure 11. (a) Cyclic voltammogram of $(NMe_4)[Ni(dtdt)_2]$ (10^{-3} M) in $CH_3CN/(NMe_4)BF_4$ (10^{-1} M) at a Pt electrode (1 mm) with a scan rate of 0.1 V s^{-1} [potential in volts *vs* Ag/AgCl (* starting potential)]. (b) Cyclic voltammogram at a Pt electrode (100 μm) with a scan rate of 800 V s^{-1}. (c) Linear voltammogram of $(NMe_4)[Ni(dtdt)_2]$ (10^{-3} M) in $CH_3CN/(NMe_4)BF_4$ (10^{-1} M) at a Pt electrode (2 mm) with a scan rate of 5 mV s^{-1} [potential in volts *vs* Ag/AgCl]. (d) Cyclic voltammogram of $(NMe_4)[Ni(dtdt)_2]$ (7×10^{-4} M) in $C_6H_5CN/(NMe_4)BF_4$ (10^{-1} M) at a Pt electrode (0.5 mm) with a scan rate of 0.1 V s^{-1} [potential in volts *vs* Ag/AgCl (* starting potential)].

Table 12. Selected Bond Distances and Angles (deg) for $[Pt(dddt)_2][Ni(dmit)_2]_2$ (**4**)

Pt(1)−S(11)	2.244(3)	S(3)−C(1)	1.74(2)	S(8)−C(4)	1.76(1)	S(12)−C(8)	1.77(3)
Ni(1)−S(1)	2.140(4)	S(3)−C(3)	1.73(2)	S(8)−C(6)	1.73(2)	S(12)−C(9)	1.83(3)
Ni(1)−S(2)	2.135(4)	S(4)−C(2)	1.72(1)	S(9)−C(5)	1.71(1)	C(1)−C(2)	1.38(2)
Ni(1)−S(6)	2.128(4)	S(4)−C(3)	1.75(2)	S(9)−C(6)	1.75(1)	C(4)−C(5)	1.43(2)
Ni(1)−S(7)	2.132(4)	S(5)−C(3)	1.61(2)‘	S(10)−C(6)	1.59(2)	C(7)−C(7)	1.40(2)
S(1)−C(1)	1.68(2)	S(6)−C(4)	1.64(2)	S(11)−C(7)	1.685(9)	C(8)−C(9)	1.56(3)
S(2)−C(2)	1.69(2)	S(7)−C(5)	1.66(1)	S(12)−C(7)	1.7343(9)		

S(11)−Pt(1)−S(11)	92.1(1)	Pt(1)−S(11)−C(7)	105.5(4)	S(6)−C(4)−C(5)	122.2(11)
S(1)−Ni(1)−S(2)	93.1(2)	C(7)−S(12)−C(8)	103.3(10)	S(8)−C(4)−C(5)	113.3(11)
S(6)−Ni(1)−S(7)	93.0(2)	C(7)−S(12)−C(9)	107.4(10)	S(7)−C(5)−C(4)	117.9(11)
Ni(1)−S(1)−C(1)	102.3(6)	S(1)−C(1)−C(2)	121.7(12)	S(9)−C(5)−C(4)	116.4(11)
Ni(1)−S(2)−C(2)	102.9(5)	S(3)−C(1)−C(2)	115.8(11)	S(8)−C(6)−S(9)	112.2(9)
C(1)−S(3)−C(3)	98.0(7)	S(2)−C(2)−S(4)	124.0(9)	S(8)−C(6)−S(10)	123.5(9)
C(2)−S(4)−C(3)	97.8(8)	S(2)−C(2)−C(1)	119.9(11)	S(9)−C(6)−S(10)	124.3(10)
Ni(1)−S(6)−C(4)	102.8(6)	S(4)−C(2)−C(1)	116.0(12)	S(11)−C(7)−C(7)	120.6(4)
Ni(1)−S(7)−C(5)	104.1(5)	S(3)−C(3)−S(4)	112.4(9)	S(12)−C(7)−C(7)	125.3(3)
C(4)−S(8)−C(6)	99.2(7)	S(3)−C(3)−S(5)	123.6(10)	S(12)−C(8)−C(9)	110.5(18)
C(5)−S(9)−C(6)	98.9(7)	S(4)−C(3)−S(5)	124.0(11)	S(12)−C(9)−C(8)	114.3(20)

is not very favorable for high conductivity and explains the low value of the measured powder conductivity for this compound (5×10^{-5} S cm^{-1}). It is interesting to note that **4** is one of the rare donor−acceptor compounds[8] in which both the donor and acceptor molecules are transition metal complexes. Even in the present case, both donor and acceptor are complexes of 1,2-dithiolate ligands.

(PPN)[M(dmit)$_2$]$_z$ and (BTP)[M(dmit)$_2$]$_z$ Compounds. The results of the electrochemical studies discussed earlier clearly show that the (cation)[M(dmit)$_2$] complexes studied may be used for the preparation of (cation)[Ni(dmit)$_2$]$_z$ NIOS radical anion salts. (PPN)[M(dmit)$_2$]$_n$ complexes with M = Te, Se and n = 2, 1 have been previously reported,[58] but no derived NIOS compounds. The (TTP)[Ni(dmit)$_2$]$_3$ (TTP^+ = tetraphenylphosphonium) radical anion salt has been reported very recently.[59]

In this work, plate-shaped crystals of the (PPN)[M(dmit)$_2$]$_z$ and (BTP)[M(dmit)$_2$]$_z$ radical anion salts with M = Ni, Pd have been prepared by galvanostatic electrolysis of solutions of the monovalent (PPN)[M(dmit)$_2$] and (BTP)[M(dmit)$_2$] complexes in acetone, acetonitrile, or 1,1,2-trichloroethane. Elemental analyses are compatible with a (cation)[M(dmit)$_2$]$_z$ stoichiometry with $z \approx 3$. This was confirmed in the case of (BTP)[Ni(dmit)$_2$]$_3$ (**5**), for which crystal quality was sufficient for an X-ray structure determination.

The asymmetric unit of (BTP)[Ni(dmit)$_2$]$_3$ (**5**) contains three crystallographically independent [Ni(dmit)$_2$] entities and one BTP^+ cation. Selected bond lengths and angles are listed in Table 13. The averaged Ni−S, inner S−C, and C=C bond lengths [2.162, 1.707, and 1.39 Å for the Ni(1) unit, 2.155, 1.697, and 1.392 Å for the Ni(2) unit, and 2.147, 1.703, and 1.387 Å for the Ni(3) unit] do not show significant differences between the three independent [Ni(dmit)$_2$] units. From this observation, it can be anticipated that the negative charge is totally delocalized over the three [Ni(dmit)$_2$] units. The almost planar [Ni(dmit)$_2$] units form stacks along the [102] direction (Figure 13) separated by the BTP^+ cations, which are located close to the external sulfur atoms of the thione group of the

(58) Singh, D. J.; Singh, H. B. *Polyhedron* **1993**, *12*, 2849.
(59) Nakamura, T.; Underhill, A. E.; Coomber, A. T.; Friend, R. H.; Tajima, H.; Kobayashi, A.; Kobayashi, H. *Inorg. Chem.* **1995**, *34*, 870.

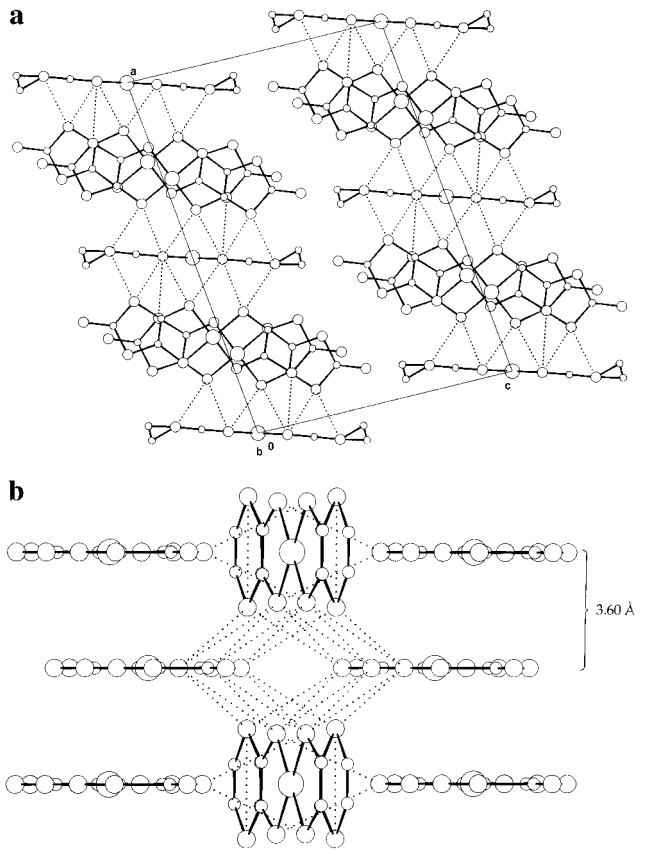

Figure 12. $[Pt(dddt)_2][Ni(dmit)_2]_2$ (**4**): (a) projection onto the *ac* plane; (b) stacking arrangement [dotted lines represent the S···S distances shorter than the sum of the van der Waals radii (3.70 Å)].

$[Ni(dmit)_2]$ units. The repeat unit along a stack is characterized by three interplanar distances of 3.59, 3.59, and 3.54 Å (Figure 13) and three modes of overlap pictured in Figure 14; two of them result from mainly longitudinal and slightly transverse offsets, resulting in reduced π interactions along the stacks.[60] In the same way, most of the short ($\leq$3.7 Å) S···S contacts occur between molecules belonging to adjacent stacks (Figure 13).

It is interesting to note that the structural arrangement of **5** is totally different from that observed for the parent compound $(TTP)[Ni(dmit)_2]_3$, which also has a phosphonium countercation (tetraphenylphosphonium instead of benzyltriphenylphosphonium) and the same 1/3 stoichiometry.[59] In $(TTP)[Ni(dmit)_2]_3$, two $Ni(dmit)_2$ units form stacks along the [010] direction, and another $Ni(dmit)_2$ unit is almost perpendicular to the stacks.[59]

The single-crystal conductivity of $(BTP)[Ni(dmit)_2]_3$ (**5**) is modest (0.2 S cm^{-1}) compared to that of $(BTP)[Pd(dmit)_2]_z$ (80 S cm^{-1}), $(PPN)[Ni(dmit)_2]_z$ (45 S cm^{-1}), and $(PPN)[Pd(dmit)_2]_z$ (62 S cm^{-1}). All of these compounds behave as semiconductors (supplementary material, Figure S2). The activation energy of $(PPN)[Ni(dmit)_2]_z$ is rather small ($\approx$0.05 eV), resulting in a high residual conductivity at low temperature (0.15 S cm^{-1} at 70 K).

$(SMe_yEt_{3-y})[M(dmit)_2]_z$ Compounds. The preparation of $(SMe_3)[Ni(dmit)_2]_2$ has been mentioned previously,[61] and $(SMe_3)[Au(dmit)_2]_z$ and $(SBu_3)[Au(dmit)_2]_z$ phases have been reported to exhibit high metal-like conductivities.[62] We have prepared all the members of the $(SMe_yEt_{3-y})[M(dmit)_2]_z$ series (with y = 0, 1, 2, 3 and M = Ni, Pd) by galvanostatic electrolysis of solutions of the monovalent $(SMe_yEt_{3-y})[Ni(dmit)_2]$ complexes and the divalent $(SMe_yEt_{3-y})_2[Pd(dmit)_2]$ complexes (the corresponding monovalent palladium complexes could not be isolated, *vide supra*) in mixtures of acetonitrile and ethyl alcohol or acetone.

The quality of the needle-shaped crystals of $(SMe_3)[Ni(dmit)_2]_2$ (**6**) was sufficient for X-ray structure determination. The unit cell parameters (space group $P\bar{1}$, a = 7.882(1) Å, b = 11.603(2) Å, c = 17.731(2) Å, α = 77.44(1)°, β = 85.86(1)°, γ = 81.27(1)°, Z = 2) were found to be equivalent to those previously reported.[61,63] Selected bond lengths and angles are listed in Table 14. The $(SMe_3)^+$ cations are statistically distributed between two positions related by a center of symmetry. The $Ni(dmit)_2$ units stack along the [100] direction. The stacking arrangement is shown in Figure 15a. Within these stacks, the interplanar distances are alternately 3.49 and 3.61 Å (Figure 15b). These stacks form layers parallel to the (001) plane and these layers alternate with the $(SMe_3)^+$ cations layers along the [001] direction. As are usually observed in $M(dmit)_2$ compounds, a number of S···S interatomic distances shorter than the sum of the van der Waals radii (3.70 Å) are observed between molecules belonging to adjacent stacks (Figure 15a).

The room temperature conductivity of the needle-shaped crystals of $(SMe_3)[Ni(dmit)_2]_2$ is 0.15 S cm^{-1}, and the compound behaves as a semiconductor with an activation energy of 0.12 eV (supplementary material, Figure S3). The room temperature conductivity of the needle-shaped crystals of $(SMeEt_2)[Ni(dmit)_2]_z$ is also moderate (0.6 S cm^{-1}), and this compound is also a semiconductor with an activation energy of 0.11 eV. The room temperature conductivity of the plate-shaped crystals of $(SEt_3)[Ni(dmit)_2]_z$ is somewhat higher (10 S cm^{-1}). It is also a semiconductor. Two regimes are observed in the temperature dependence of the conductivity with activation energies of 0.05 eV from 300 to 220 K and 0.18 eV from 220 to 115 K.

The unit cell of $(SMeEt_2)[Pd(dmit)_2]_2$ (**7**) contains two crystallographically independent $Pd(dmit)_2$ units and one $(SMeEt_2)^+$ cation. Selected bond distances and angles are given in Table 15. Within the esds, the averaged intramolecular distances are almost identical in both $Pd(dmit)_2$ units. Each $Pd(dmit)_2$ unit forms segregated stacks along the [100] direction (Figure 16a). The stacks formed by one of the independent $Pd(dmit)_2$ unit are connected to the stacks formed by the other independent $Pd(dmit)_2$ unit through its terminal sulfur atoms along the [010] direction. In a stack, the $Pd(dmit)_2$ entities are paired, forming $[Pd(dmit)_2]_2$ dimers with a Pd−Pd bond length of 3.131(2) and 3.138(2) Å. Thus, the structure consists of layers of $[Pd(dmit)_2]_2$ dimers parallel to the *ac* plane, connected to each other through short S···S contacts (Figure 16b) and separated by sheets of $(SMeEt_2)^+$ cations. The $Pd(dmit)_2$ entities are eclipsed within a dimer and slipped between dimers, with interplanar distances of 3.50 and 3.59 Å, respectively (Figure 16c).

By contrast with $(SMe_3)[Ni(dmit)_2]_2$, the room temperature conductivity of the plate-shaped crystals of $(SMeEt_2)[Pd(dmit)_2]_2$ is very high (100 S cm^{-1}). The temperature dependence of the

(60) Kobayashi, A.; Kim, A.; Sasaki, H.; Kato, R.; Kobayashi, H. *Solid State Commun.* **1987**, *62*, 57.
(61) Kato, R.; Kobayashi, H.; Kim, H.; Kobayashi, A.; Sasaki, Y.; Mori, T.; Inokuchi, H. *Synth. Metals* **1988**, *27B*, 359.
(62) Yagubskii, E. B.; Ukhin, L. Yu.; Kotov, A. I. *Dokl. An. SSSR* **1986**, *290*, 115.
(63) Kobayashi *et al.* have reported in ref 61 the following unit cell parameters for $(SMe_3)[Ni(dmit)_2]_2$: space group $P\bar{1}$, a = 20.330(1) Å, b = 11.598(5) Å, c = 7.883(4) Å, α = 98.62(4)°, β = 111.14(5)°, γ = 108.81(5)°, Z = 2). During the writing of this manuscript, we became aware that the structure of this compound had been solved simultaneously by Liu *et al.* (Liu, H. L.; Tanner, D. B.; Pullen, A. E.; Abboud, K. A.; Reynolds, J. R. Personal communication, submitted for publication in *Phys. Rev. B*). They report the following unit cell parameters: space group $P\bar{1}$, a = 7.923(1) Å, b = 11.647(5) Å, c = 17.812(2) Å, α = 77.46(1)°, β = 85.93(1)°, γ = 81.36(1)°, Z = 2. The main features of this structure are essentially similar to those reported in the present work.

Table 13. Selected Bond Distances and Angles (deg) for (BTP)[Ni(dmit)$_2$]$_3$ (**5**)

Ni(1)−S(1)	2.154(2)	S(3)−C(3)	1.732(7)	S(14)−C(8)	1.733(7)	S(24)−C(15)	1.749(8)
Ni(1)−S(2)	2.161(2)	S(4)−C(2)	1.725(6)	S(14)−C(9)	1.730(8)	S(25)−C(15)	1.608(8)
Ni(1)−S(6)	2.163(2)	S(4)−C(3)	1.738(7)	S(15)−C(9)	1.634(8)	S(26)−C(16)	1.693(7)
Ni(1)−S(7)	2.168(2)	S(5)−C(3)	1.632(7)	S(16)−C(10)	1.697(7)	S(27)−C(17)	1.707(7)
Ni(2)−S(11)	2.156(2)	S(6)−C(4)	1.703(7)	S(17)−C(11)	1.685(6)	S(28)−C(16)	1.734(7)
Ni(2)−S(12)	2.158(2)	S(7)−C(5)	1.712(7)	S(18)−C(10)	1.739(7)	S(28)−C(18)	1.729(8)
Ni(2)−S(16)	2.159(2)	S(8)−C(4)	1.729(7)	S(18)−C(12)	1.739(7)	S(29)−C(17)	1.730(7)
Ni(2)−S(17)	2.148(2)	S(8)−C(6)	1.735(8)	S(19)−C(11)	1.730(6)	S(29)−C(18)	1.727(8)
Ni(3)−S(21)	2.153(2)	S(9)−C(5)	1.723(7)	S(19)−C(12)	1.737(7)	S(30)−C(18)	1.629(8)
Ni(3)−S(22)	2.145(2)	S(9)−C(6)	1.725(8)	S(20)−C(12)	1.626(7)	C(1)−C(2)	1.386(9)
Ni(3)−S(26)	2.148(2)	S(10)−C(6)	1.642(8)	S(21)−C(13)	1.693(7)	C(4)−C(5)	1.40(1)
Ni(3)−S(27)	2.141(2)	S(11)−C(7)	1.698(7)	S(22)−C(14)	1.677(7)	C(7)−C(8)	1.390(9)
S(1)−C(1)	1.704(6)	S(12)−C(8)	1.707(7)	S(23)−C(13)	1.729(7)	C(10)−C(11)	1.394(9)
S(2)−C(2)	1.708(6)	S(13)−C(7)	1.734(7)	S(23)−C(15)	1.750(8)	C(13)−C(14)	1.405(9)
S(3)−C(1)	1.731(7)	S(13)−C(9)	1.752(8)	S(24)−C(14)	1.727(7)	C(16)−C(17)	1.369(9)

S(1)−Ni(1)−S(2)	92.68(7)	C(13)−S(23)−C(15)	97.6(3)	S(13)−C(9)−S(14)	112.8(4)
S(6)−Ni(1)−S(7)	93.06(8)	C(14)−S(24)−C(15)	97.9(3)	S(13)−C(9)−S(15)	123.5(5)
S(11)−Ni(2)−S(12)	93.18(7)	Ni(3)−S(26)−C(16)	102.4(2)	S(14)−C(9)−S(15)	123.6(5)
S(16)−Ni(2)−S(17)	92.81(7)	Ni(3)−S(27)−C(17)	102.7(2)	S(16)−C(10)−C(11)	120.8(5)
S(21)−Ni(3)−S(22)	92.99(7)	C(16)−C(28)−C(18)	97.0(4)	S(18)−C(10)−C(11)	115.8(5)
S(26)−Ni(3)−S(27)	93.15(7)	C(17)−C(29)−C(18)	96.7(4)	S(17)−C(11)−C(10)	120.6(5)
Ni(1)−S(1)−C(1)	103.1(2)	S(1)−C(1)−C(2)	120.8(5)	S(19)−C(11)−C(10)	115.7(5)
Ni(1)−S(2)−C(2)	103.0(2)	S(3)−C(1)−C(2)	116.0(5)	S(18)−C(12)−S(19)	113.2(4)
C(1)−S(3)−C(3)	97.3(3)	S(2)−C(2)−C(1	120.3(5)	S(18)−C(12)−S(20)	123.5(4)
C(2)−S(4)−C(3)	97.3(3)	S(4)−C(2)−C(1)	116.0(5)	S(19)−C(12)−S(20)	123.3(4)
Ni(1)−S(6)−C(4)	102.7(2)	S(3)−C(3)−S(4)	113.4(4)	S(21)−C(13)−C(14)	120.3(5)
Ni(1)−S(7)−C(5)	102.8(2)	S(3)−C(3)−S(5)	123.3(4)	S(23)−C(13)−C(14)	116.1(5)
C(4)−S(8)−C(6)	97.8(4)	S(4)−C(3)−S(5)	123.3(4)	S(22)−C(14)−C(13)	120.8(5)
C(5)−S(9)−C(6)	97.5(4)	S(6)−C(4)−C(5)	121.3(5)	S(24)−C(14)−C(13)	115.7(5)
Ni(2)−S(11)−C(7)	102.8(2)	S(8)−C(4)−C(5)	114.8(5)	S(23)−C(15)−S(24)	112.7(4)
Ni(2)−S(12)−C(8)	102.4(2)	S(7)−C(5)−C(4)	120.1(5)	S(23)−C(15)−S(25)	124.5(5)
C(7)−S(13)−C(9)	97.4(3)	S(9)−C(5)−C(4)	116.4(5)	S(24)−C(15)−S(25)	122.8(5)
C(8)−S(14)−C(9)	97.9(3)	S(8)−C(6)−S(9)	113.4(4)	S(26)−C(16)−C(17)	121.5(5)
Ni(2)−S(16)−C10)	102.5(2)	S(8)−C(6)−S(10)	122.7(5)	S(28)−C(16)−C(17)	115.6(5)
Ni(2)−S(17)−C(11)	103.3(2)	S(9)−C(6)−S(10)	123.9(5)	S(27)−C(17)−C(16)	120.2(5)
C(10)−S(18)−C(12)	97.5(3)	S(11)−C(7)−C(8)	120.8(5)	S(29)−C(17)−C(16)	116.7(5)
C(11)−S(19)−C(12)	97.9(3)	S(13)−C(7)−C(8)	115.8(5)	S(28)−C(18)−S(29)	113.8(4)
Ni(3)−S(21)−C(13)	102.7(2)	S(12)−C(8)−C(7)	120.8(5)	S(28)−C(18)−S(30)	123.8(5)
Ni(3)−S(22)−C(14)	103.2(2)	S(14)−C(8)−C(7)	115.8(5)	S(29)−C(18)−S(30)	122.4(5)

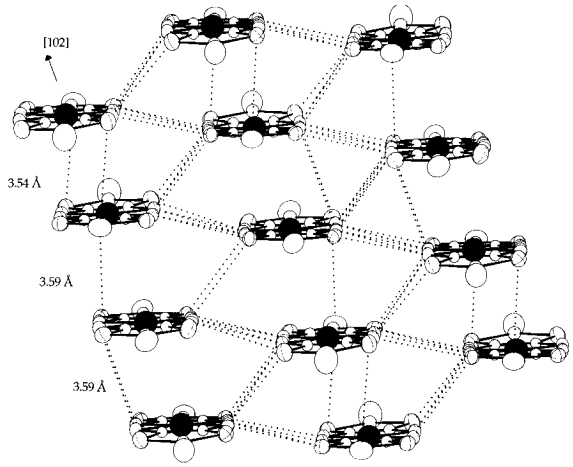

Figure 13. (BTP)[Ni(dmit)$_2$]$_3$ (**5**): stacking of the Ni(dmit)$_2$ entities along [102].

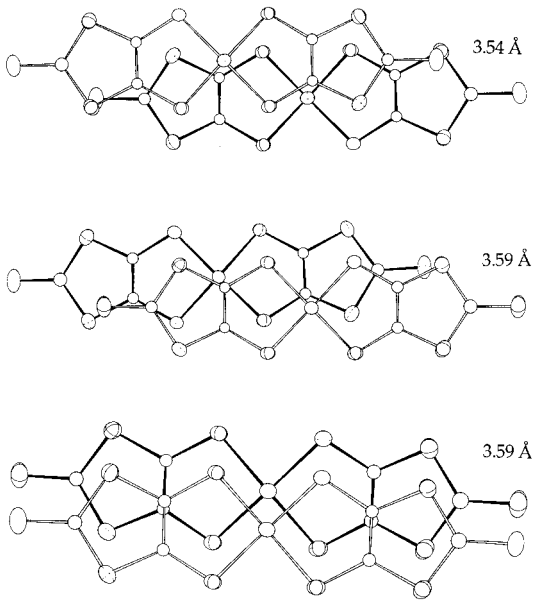

Figure 14. Different modes of molecular overlap within the Ni(dmit)$_2$ stacks of (BTP)[Ni(dmit)$_2$]$_3$ (**5**).

conductivity of this compound is shown in Figure 17. The behavior is that of a pseudometal from 300 down to 150 K and increases slightly up to 108 S cm^{-1}. At ≈150 K, the compound undergoes a transition to a semiconducting state. However, this behavior is not reversible when heating back to room temperature and on subsequent cooling cycles, whereby the compound remains semiconducting over the whole temperature range. This behavior is reminiscent of that of the superconducting α-(TTF)-[Pd(dmit)$_2$]$_2$ phase.[19c]

Electronic Structure of (SMeEt$_2$)[Pd(dmit)$_2$]$_2$. Despite the similarities in resistivity behavior between (SMeEt$_2$)[Pd(dmit)$_2$]$_2$ and α-(TTF)[Pd(dmit)$_2$]$_2$,[19c] there are two subtle but important differences in the structure of the acceptor layers of these salts.[19c,20] First, the Pd(dmit)$_2$ stacks are uniform in the latter, but contain [Pd(dmit)$_2$]$_2$ diads in the former. Second, the two acceptor layers of the unit cell in α-(TTF)[Pd(dmit)$_2$]$_2$ are related by a symmetry element and thus are equivalent, whereas in (SMeEt$_2$)[Pd(dmit)$_2$]$_2$ the unit cell contains two crystallographically independent Pd(dmit)$_2$ units.

The calculated band structures for the two different acceptor layers of (SMeEt$_2$)[Pd(dmit)$_2$]$_2$ are shown in Figure 18. The

Table 14. Selected Bond Distances and Angles (deg) for $(SMe_3)[Ni(dmit)_2]_2$ (**6**)

Ni(1)−S(1)	2.153(2)	S(2)−C(2)	1.686(7)	S(5)−C(3)	1.650(8)	S(9)−C(5)	1.746(8)
Ni(1)−S(2)	2.151(2)	S(3)−C(1)	1.729(7)	S(6)−C(4)	1.695(8)	S(9)−C(6)	1.733(7)
Ni(1)−S(6)	2.163(2)	S(3)−C(3)	1.721(8)	S(7)−C(5)	1.691(7)	S(10)−C(6)	1.648(8)
Ni(1)−S(7)	2.162(2)	S(4)−C(2)	1.723(8)	S(8)−C(4)	1.742(7)	C(1)−C(2)	1.388(8)
S(1)−C(1)	1.693(7)	S(4)−C(3)	1.717(7)	S(8)−C(6)	1.724(8)	C(4)−C(5)	1.38(1)
Ni(11)−S(11)	2.152(2)	S(12)−C(12)	1.709(7)	S(15)−C(13)	1.659(8)	S(19)−C(15)	1.746(7)
Ni(11)−S(12)	2.158(2)	S(13)−C(11)	1.735(7)	S(16)−C(14)	1.688(7)	S(19)−C(16)	1.725(7)
Ni(11)−S(16)	2.154(2)	S(13)−C(13)	1.706(9)	S(17)−C(15)	1.689(7)	S(20)−C(16)	1.637(8)
Ni(11)−S(17)	2.161(2)	S(14)−C(12)	1.736(8)	S(18)−C(14)	1.735(7)	C(11)−C(12)	1.360(9)
S(11)−C(11)	1.700(8)	S(14)−C(13)	1.730(7)	S(18)−C(16)	1.731(8)	C(14)−C(15)	1.366(9)

S(1)−Ni(1)−S(2)	92.63(7)	C(4)−S(8)−C(6)	97.6(3)	S(4)−C(3)−S(5)	122.7(5)
S(6)−Ni(1)−S(7)	93.09(7)	C(5)−S(9)−C(6)	97.8(4)	S(6)−C(4)−C(5)	120.8(5)
Ni(1)−S(1)−C(1)	102.9(2)	S(1)−C(1)−C(2)	120.5(5)	S(8)−C(4)−C(5)	116.2(6)
Ni(1)−S(2)−C(2)	103.0(2)	S(3)−C(1)−C(2)	116.1(5)	S(7)−C(5)−C(4)	122.0(6)
C(1)−S(3)−C(3)	96.6(3)	S(2)−C(2)−C(1)	120.9(6)	S(9)−C(5)−C(4)	115.1(5)
C(2)−S(4)−C(3)	97.1(3)	S(4)−C(2)−C(1)	115.6(5)	S(8)−C(6)−S(9)	113.2(4)
Ni(1)−S(6)−C(6)	102.2(2)	S(3)−C(3)−S(4)	114.5(4)	S(8)−C(6)−S(10)	124.2(4)
Ni(1)−S(7)−C(5)	101.9(3)	S(3)−C(3)−S(5)	122.7(4)	S(9)−C(6)−S(10)	122.6(5)
S(11)−Ni(11)−S(12)	93.49(7)	C(15)−S(19)−C(16)	97.3(3)	S(16)−C(14)−C(15)	121.0(5)
S(16)−Ni(11)−S(17)	92.97(7)	S(11)−C(11)−C(12)	121.5(5)	S(18)−C(14)−C(15)	116.2(5)
Ni(11)−S(11)−C(11)	102.0(2)	S(13)−C(11)−C(12)	115.7(6)	S(17)−C(15)−C(14)	121.9(6)
Ni(11)−S(12)−C(12)	101.6(2)	S(12)−C(12)−C(11)	121.3(6)	S(19)−C(15)−C(14)	115.6(5)
C(11)−S(13)−C(13)	97.4(3)	S(14)−C(12)−C(11)	116.3(5)	S(18)−C(16)−S(19)	113.4(4)
C(12)−S(14)−C(13)	96.6(4)	S(13)−C(13)−S(14)	114.0(5)	S(18)−C(16)−S(20)	121.9(4)
Ni(11)−S(16)−C(14)	102.3(2)	S(13)−C(13)−S(15)	123.6(4)		
Ni(11)−S(17)−C(15)	101.7(2)	S(14)−C(13)−S(15)	122.4(5)		

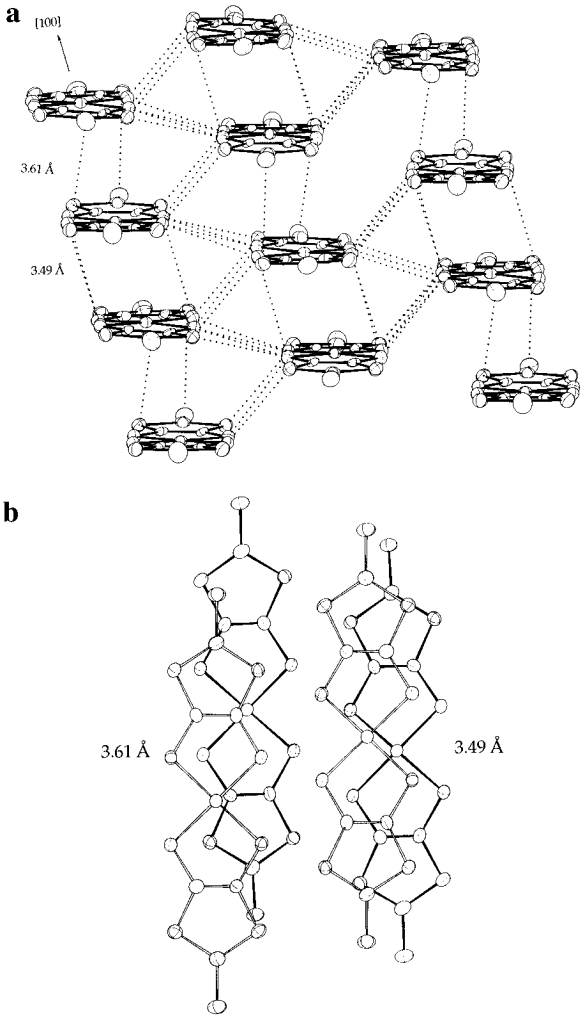

Figure 15. $(SMe_3)[Ni(dmit)_2]_2$ (**6**): (a) stacking of the $Ni(dmit)_2$] units along the [100] direction with the network of S···S distances shorter than the sum of the van der Waals radii (3.70 Å) (dotted lines); (b) the two different modes of molecular overlap within the $Ni(dmit)_2$ stacks.

bands for the layer containing diads with a Pd···Pd bond length of 3.131(2) Å (layer 1) are shown as continuous lines; those for the layer containing diads with a Pd···Pd bond length of 3.138(2) Å (layer 2) are shown as dashed lines. As usual, in $M(dmit)_2$ salts with strong dimerization,[64−67] the lowest combination of the two $Pd(dmit)_2$ LUMOs (Ψ^+_{LUMO}) is lower in energy than the highest combination of the two $Pd(dmit)_2$ HOMOs (Ψ^-_{HOMO}). The intermolecular interactions within the two acceptor slabs of $(SMeEt_2)[Pd(dmit)_2]_2$ do not change this level ordering, so that the third pair of bands from the bottom of Figure 18, *i.e.*, the bands that are partially filled, is the Ψ^-_{HOMO} bands.

Since there is a short interlayer S···S contact in $(SMeEt_2)$-$[Pd(dmit)_2]_2$, we have also carried out calculations for the three-dimensional acceptor lattice. However, the band dispersion along the interlayer direction is very small, and the calculated 3D band structure is practically the superposition of the band structures of the two slabs. Consequently, from now on, our discussion will be based on the results of Figure 18. The most interesting result of this band structure is that the bands of layer 2 are always at slightly lower energies than those of layer 1. Consequently, the filling of the partially filled band of layers 1 and 2, *i.e.*, the associated charge transfer, must be different. According to our calculations, the number of electrons transferred per $Pd(dmit)_2$ unit (ρ) is approximately $^1/_3$ for layer 1 and $^2/_3$ for layer 2. The two partially filled bands of Figure 18 are completely parallel and shifted by ≈0.08 eV. Thus, the interdiad interactions in both layers must be almost identical and are not at the origin of the different charge transfer. The energy difference between the HOMOs of the $Pd(dmit)_2$ molecules in both layers is 0.095 eV, with the energy of the HOMOs of the $Pd(dmit)_2$ in layer 2 being lower. The splitting between the two HOMO levels of the diads (Ψ^+_{HOMO} and Ψ^-_{HOMO}) in both layers differs by only 0.008 eV. Consequently, the difference between the partially filled bands of both layers originates from slight geometrical differences between the corresponding $Pd(dmit)_2$ molecules. This somewhat surprising difference in the charge transfer for the two layers, which is not revealed by important geometrical differences, is due to the nonexistence of a symmetry element relating both layers. Given the accuracy of the crystal structure, the $^2/_3$ and $^1/_3$ values for ρ evidently should be taken as indicative, and their difference can be considered an upper limit.

Table 15. Selected Bond Distances and Angles (deg) for $(SMeEt_2)[Pd(dmit)_2]_2$ (**7**)

Pd(1)−Pd(1)	3.131(2)	S(12)−C(12)	1.70(1)	S(19)−C(16)	1.75(2)	S(28)−C(24)	1.73(1)
Pd(1)−S(11)	2.305(4)	S(13)−C(11)	1.73(1)	S(20)−C(16)	1.62(2)	S(28)−C(26)	1.74(2)
Pd(1)−S(12)	2.289(3)	S(13)−C(13)	1.74(2)	S(21)−C(21)	1.71(1)	S(29)−C(25)	1.74(1)
Pd(1)−S(16)	2.283(4)	S(14)−C(12)	1.73(1)	S(22)−C(22)	1.69(1)	S(29)−C(26)	1.72(2)
Pd(1)−S(17)	2.293(3)	S(14)−C(13)	1.72(2)	S(23)−C(21)	1.75(1)	S(30)−C(26)	1.64(2)
Pd(2)−Pd(2)	3.138(2)	S(15)−C(13)	1.63(2)	S(23)−C(23)	1.74(1)	C(11)−C(12)	1.39(2)
Pd(2)−S(21)	2.296(3)	S(16)−C(14)	1.69(1)	S(24)−C(22)	1.73(1)	C(14)−C(15)	1.38(2)
Pd(2)−S(22)	2.287(4)	S(17)−C(15)	1.69(1)	S(24)−C(23)	1.71(1)	C(21)−C(22)	1.35(2)
Pd(2)−S(26)	2.288(4)	S(18)−C(14)	1.71(1)	S(25)−C(23)	1.64(1)	C(24)−C(25)	1.37(2)
Pd(2)−S(27)	2.295(4)	S(18)−C(16)	1.70(1)	S(26)−C(24)	1.70(1)		
S(11)−C(11)	1.68(1)	S(19)−C(15)	1.75(1)	S(27)−C(25)	1.71(1)		

S(11)−Pd(1)−S(12)	89.9(1)	C(21)−S(23)−C(23)	96.0(7)	S(19)−C(15)−C(14)	115.1(11)
S(16)−Pd(1)−S(17)	89.8(1)	C(22)−S(24)−C(23)	97.8(7)	S(18)−C(16)−S(19)	112.9(8)
Pd(2)−Pd(2)−S(21)	91.6(1)	Pd(2)−S(26)−C(24)	102.1(5)	S(18)−C(16)−S(20)	124.9(10)
Pd(2)−Pd(2)−S(22)	92.0(1)	Pd(2)−S(27)−C(25)	101.0(5)	S(19)−C(16)−S(20)	122.1(9)
S(21)−Pd(2)−S(22)	89.8(1)	C(24)−S(28)−C(26)	97.6(7)	S(21)−C(21)−C(22)	124.4(10)
Pd(2)−Pd(2)−S(26)	91.5(1)	C(25)−S(29)−C(26)	97.7(7)	S(23)−C(21)−C(22)	116.6(11)
Pd(2)−Pd(2)−S(27)	91.9(1)	S(1)−C(2)−C(3)	108.9(24)	S(22)−C(22)−C(21)	123.2(11)
S(26)−Pd(2)−S(27)	90.1(1)	S(1)−C(4)−C(5)	106.5(21)	S(24)−C(22)−C(21)	115.9(10)
Pd(1)−S(11)−C(11)	101.4(5)	S(11)−C(11)−C(12)	124.4(10)	S(23)−C(23)−S(24)	113.4(8)
Pd(1)−S(12)−C(12)	102.0(4)	S(13)−C(11)−C(12)	114.2(10)	S(23)−C(23)−S(25)	121.7(8)
C(11)−S(13)−C(13)	98.8(7)	S(13)−C(12)−C(11)	122.3(10)	S(24)−C(23)−S(25)	124.6(9)
C(12)−S(14)−C(13)	98.0(7)	S(14)−C(12)−C(11)	116.7(10)	S(26)−C(24)−C(25)	122.3(10)
Pd(1)−S(16)−C(14)	102.8(5)	S(13)−C(13)−S(14)	112.4(9)	S(28)−C(24)−C(25)	115.9(10)
Pd(1)−S(17)−C(15)	101.0(5)	S(13)−C(13)−S(15)	123.3(10)	S(27)−C(25)−C(24)	124.4(10)
C(14)−S(18)−C(16)	99.0(7)	S(14)−C(13)−S(15)	124.2(10)	S(29)−C(25)−C(24)	115.7(10)
C(15)−S(19)−C(16)	96.9(7)	S(16)−C(14)−C(15)	121.6(11)	S(28)−C(26)−S(29)	113.1(9)
Pd(2)−S(21)−C(21)	100.6(5)	S(18)−C(14)−C(15)	116.0(10)	S(28)−C(26)−S(30)	122.6(10)
Pd(2)−S(22)−C(22)	101.9(5)	S(17)−C(15)−C(14)	124.7(10)	S(29)−C(26)−S(30)	124.3(10)

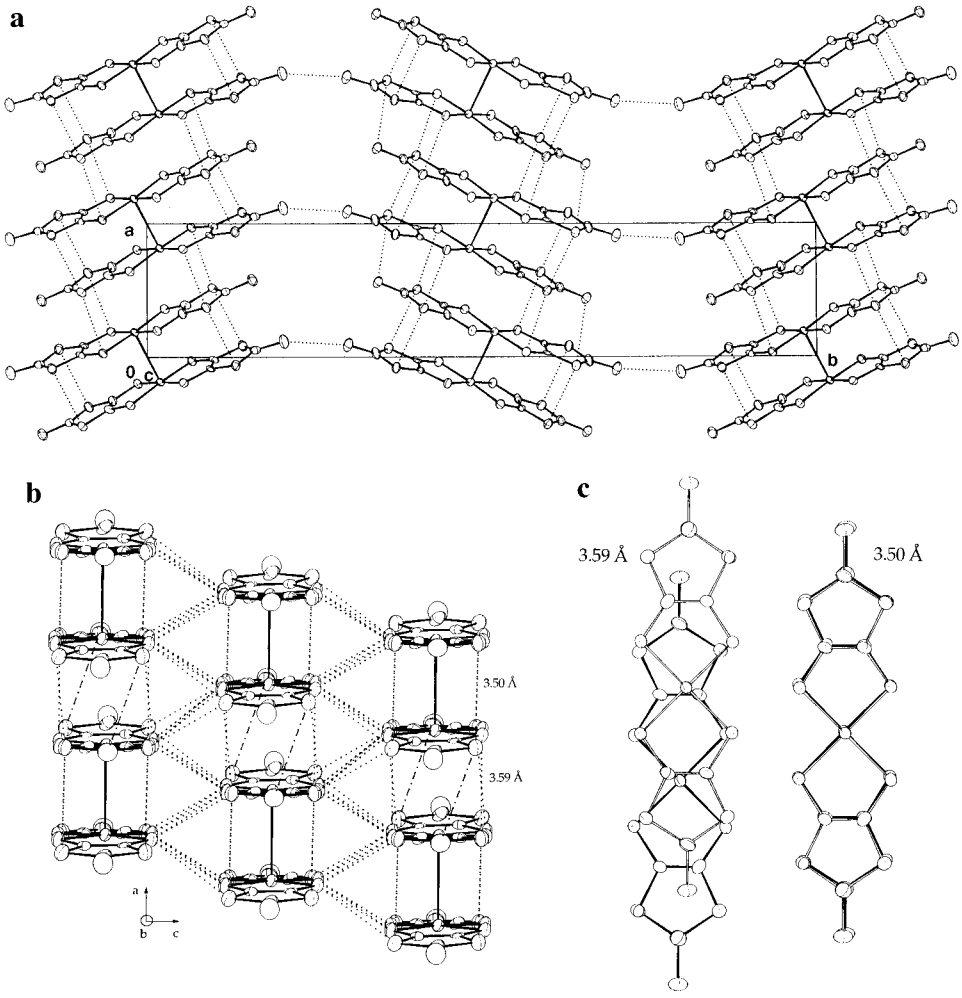

Figure 16. $(SMeEt)_2[Pd(dmit)_2]_2$ (**7**): (a) projection on the *ab* plane; (b) stacking arrangement within the Pd units [dotted lines represent the S···S distances shorter than the sum of the van der Waals radii (3.70 Å), and S···S distances represented with − · − are observed only for the Pd(1) units]; (c) the two different modes of molecular overlap within the $Pd(dmit)_2$ stacks.

Unlike in the organic systems based on TTF-like molecules where the central C═C bond length is quite a good indicator of the oxidation state of the donor, we have previously shown that the M−S bond length in $M(dmit)_2$-based systems should

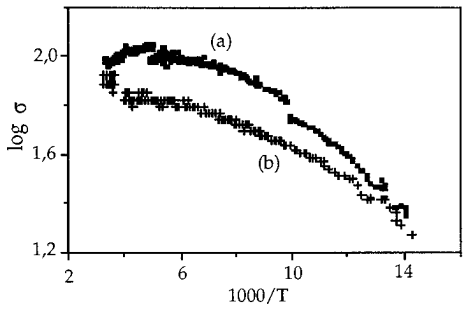

Figure 17. Temperature dependence of the conductivity of $(SMeEt)_2[Pd(dmit)_2]_2$ (**7**): (a) decreasing temperature; (b) increasing temperature.

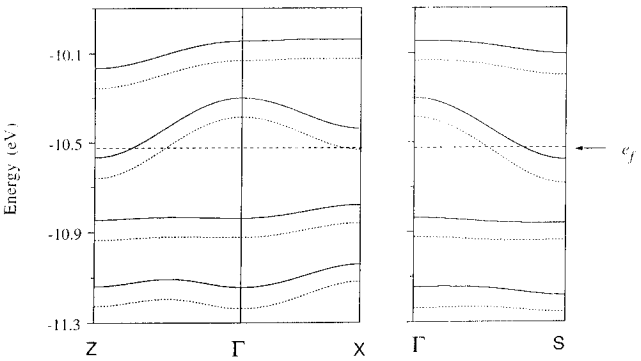

Figure 18. Dispersion relations calculated for the HOMO and LUMO bands of the two $Pd(dmit)_2$ layers in $(SMeEt_2)[Pd(dmit)_2]_2$. The bands of layer 1 (see text) are shown as continuous lines, whereas those of layer 2 are shown as dashed lines. **Γ**, **X**, **Z**, and **S** refer to the wave vectors (0, 0), (a*/2, 0), (0, c*/2), and (−a*/2, c*/2), respectively.

be quite insensitive to the oxidation state of the $M(dmit)_2$ acceptor.[47,64] Moreover, as is the case for all other metallic $Pd(dmit)_2$ layers containing diads, and as a consequence of the interdiad slipping (see Figure 16c), the dispersion of the Ψ^-_{HOMO} band along the chain direction (Γ → X in Figure 18) is not large (*i.e.*, the interdiad interactions within the chains are weaker than those along the interchain direction). Thus, a relatively small energy shift between the two Ψ^-_{HOMO} bands can lead to sizable differences in their electron filling. In addition, according to the nature of the HOMOs of $Pd(dmit)_2$, as the charge transfer toward the Ψ^-_{HOMO} band increases, the main effect should be a small shortening of the C═C bond lengths and a smaller lengthening of the inner C−S and terminal C═S bond lengths. Indeed, all of these trends may be found when comparing the geometries of the $Pd(dmit)_2$ units of layers 1 and 2 (see Table 15). Thus, we conclude that although it might be overestimated the difference in the charge transfers for the two layers is a real fact.

The calculated Fermi surfaces for layer 1 ($\rho = {}^1/_3$) and layer 2 ($\rho = {}^2/_3$) are shown in Figure 19a,b, respectively. Also shown in Figure 19c,d are the calculated Fermi surfaces assuming the same charge transfer ($\rho = {}^1/_2$) for both layers. Whereas the Fermi surface of Figure 19b is closed, all others are open. The two Fermi surfaces of Figure 19c,d are practically identical, as were the interdiad interactions in the two layers (see above). They are relatively well nested by the wave vector $\mathbf{q} \approx {}^1/_4a^* + {}^1/_2c^*$. Since a transition to a semiconducting state requires the destruction of the Fermi surfaces of both layers, it is clear that a Fermi surface instability like a charge density wave is not at the origin of the transition around 150 K (except if $\rho \approx {}^1/_2$). As the tunneling interaction between the slabs can be neglected, the real Fermi surface of the material is the superposition of those of the two layers. Consequently, above 150 K, $(SMeEt_2)$-

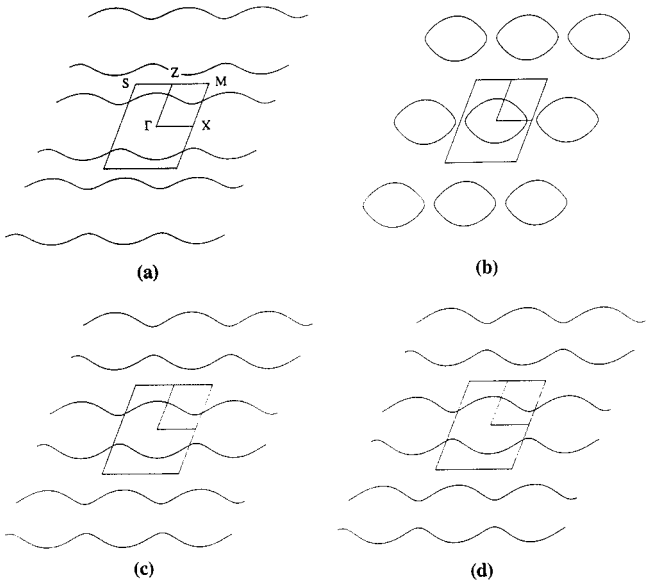

Figure 19. Calculated Fermi surfaces for the two $Pd(dmit)_2$ layers of $(SMeEt_2)[Pd(dmit)_2]_2$: (a) layer 1 and $\rho = {}^1/_3$; (b) layer 2 and $\rho = {}^2/_3$; (c) layer 1 and $\rho = 1/2$; and (d) layer 2 and $\rho = {}^1/_2$.

$[Pd(dmit)_2]_2$ should be a 2D metal (or a pseudo-2D metal depending on the charge transfer) with a better conductivity along the c direction. Moreover, the conductivity anisotropy should be larger when the difference in charge transfer between the two layers decreases.

Charge transfer salts containing $Pd(dmit)_2$ layers with $\rho \approx {}^1/_2$ may exhibit quite different properties although their structures are similar.[65,68−70] For example, whereas $Cs[Pd(dmit)_2]_2$[65] and δ-$TTF[Pd(dmit)_2]_2$[68] are metallic at room temperature, $(PMe_4)[Pd(dmit)_2]_2$[69] and β-$(NMe_4)[Pd(dmit)_2]_2$[70] are room temperature semiconductors. Moreover, even if both $Cs[Pd(dmit)_2]_2$ and δ-$TTF[Pd(dmit)_2]_2$ undergo a metal−insulator transition,[65,68] the origin of the two transitions is different. X-ray diffuse scattering studies have shown that whereas the first one is a structural Peierls type transition,[65] the second one occurs without any structural change.[71] In all of these cases, the Mott−Hubbard interactions for these salts are of the same order of magnitude as the Ψ^-_{HOMO} bandwidth, and, hence, the metallic and localized states are in strong competition.[64] This is consistent with the inversion of the Ψ^+_{LUMO} and Ψ^-_{HOMO} levels observed for all of these slabs. Thus, the interaction between the two $Pd(dmit)_2$ of the diad is strong, and, consequently, the essential building block of the slab is one such diad. If $\rho = {}^1/_2$, there is one electron per $[Pd(dmit)_2]_2$ diad, which formally corresponds to a 1/1 charge transfer salt where one electron is localized in each unit of the lattice. For $Pd(dmit)_2$ layers built from $[Pd(dmit)_2]_2$

(64) Canadell, E.; Ravy, S.; Pouget, J.-P.; Brossard, L.; Legros, J.-P. *Solid State Commun.* **1990**, *75*, 633.
(65) Underhill, A. E.; Clark, R. A.; Marsden, I.; Allan, M.; Friend, R. H.; Tajima, H.; Naito, T.; Tamura, M.; Kuroda, H.; Kobayashi, A.; Kobayashi, H.; Canadell, E.; Ravy, S.; Pouget, J.-P. *J. Phys.: Condens. Matter* **1991**, *3*, 933.
(66) Pomarède, B.; Garreau, B.; Malfant, I.; Valade, L.; Cassoux, P.; Legros, J.-P.; Audouard, A.; Brossard, L.; Ulmet, J.-P.; Doublet, M.-L.; Canadell, E. *Inorg. Chem.* **1994**, *33*, 3401.
(67) Doublet, M.-L.; Canadell, E.; Garreau, B.; Legros, J.-P.; Brossard, L.; Cassoux, P.; Pouget, J.-P. *J. Phys.: Condens. Matter* **1995**, *7*, 4673.
(68) Legros, J.-P.; Valade, L. *Solid State Commun*. **1988**, *68*, 599. Although the charge transfer in δ-$TTF[Pd(dmit)_2]_2$ has not been unequivocally demonstrated, the fact that there is no interaction among the TTF donors and their internal geometry both strongly suggest a charge transfer of one electron per TTF donor, *i.e.*, $\rho = {}^1/_2$.
(69) Faulmann, C.; Legros, J.-P.; Cassoux, P.; Cornelissen, J.; Brossard, L.; Inokuchi, M.; Tajima, H.; Tokumoto, M. *J. Chem. Soc., Dalton Trans.* **1994**, 249.
(70) Kobayashi, A.; Kim, H.; Sasaki, Y.; Murata, K.; Kato, R.; Kobayashi, H. *J. Chem. Soc., Faraday Trans.* **1990**, 361.
(71) Ravy, S. Personal communication.

diads, there should be a strong tendency for electron localization with one electron in each diad. The difference from the usual 1/1 charge transfer salts is that, since each unit of the layer contains two monomers, the intrasite electron repulsion (U) should be considerably smaller. Consequently, the localized state is not always the ground state as in 1/1 charge transfer salts, but competes with the metallic state.

It is clear that metallic charge transfer salts containing Pd(dmit)$_2$ layers built from [Pd(dmit)$_2$]$_2$ diads and with $\rho = {}^1/_2$ have a strong tendency to undergo metal−insulator transitions through either Mott−Hubbard or Fermi surface nesting mechanisms, the latter becoming less favorable when ρ becomes larger than $^1/_2$. By taking into account (i) the existence of two symmetry nonequivalent layers in (SMeEt$_2$)[Pd(dmit)$_2$]$_2$ and (ii) the activated conductivity regime below the transition temperature, it may be suggested that, whatever ρ is at higher temperature, it becomes $\approx {}^1/_2$ for both layers near 150 K. The metal−insulator transition at 150 K can be due to either localization, as presumably occurs for δ-TTF[Pd(dmit)$_2$]$_2$, or a Peierls transition as in Cs[Pd(dmit)$_2$]$_2$. Magnetic susceptibility and X-ray diffuse scattering measurements are needed (and are under progress) to clarify this point. However, the temperature dependence of the conductivity suggests that localization is more likely.

In contrast with (SMeEt$_2$)[Pd(dmit)$_2$]$_2$, the HOMO and LUMO bands of the Pd(dmit)$_2$ layers in the typically one-dimensional α-TTF[Pd(dmit)$_2$]$_2$ were found to have a strong dispersion along the stacking direction.[47] Moreover, these bands form two sets of overlapping parallel bands, which are very well nested. It is clear that the electronic structures of the α-TTF[Pd(dmit)$_2$]$_2$ and (SMeEt$_2$)[Pd(dmit)$_2$]$_2$ salts are very different, and, consequently, the reminiscence between the electrical behaviors of these two salts probably is accidental. The main reason for the contrasting band structures lies in the existence of uniform Pd(dmit)$_2$ stacks in the first salt, whereas the stacks of the second one are built from slipped [Pd(dmit)$_2$]$_2$ diads.

Conclusion

This work was part of the general research effort[4,13,14,23−25] aimed at extending the range of molecular conductors and superconductors based on transition metal complexes by (i) designing and using new ligands, (ii) changing the nature of the metal, and (iii) changing the nature of the counterion in the derived NIOS compounds.

Although the dddt^{2-} and dtdt^{2-} ligands were designed and selected because of their resemblance to the previously successfully used dmit^{2-} ligand, no radical anion NIOS compounds could be obtained by from their complexes, and only radical cation NIOS compounds may be obtained by using the complexes of dddt^{2-}. An explanation of this behavior is found in the compared electrochemical studies of the complexes of these three ligands.

Thus, the M(dmit)$_2$ complexes remain the best candidate systems for preparing conducting NIOS compounds, and several examples are given in this work. Much work remains to be done to better characterize some of the most interesting prepared phases, for example, the highly conducting phases (BTP)[Pd(dmit)$_2$]$_z$, (PPN)[Ni(dmit)$_2$]$_z$, and (PPN)[Pd(dmit)$_2$]$_z$, by determining their structures and carrying out further conductivity measurements, for example, under pressure. The continuation of this work is under way and subject to the availability of crystals of sufficient size and quality.

However, the basic question concerning the structural and electronic features that make the M(dmit)$_2$ complexes so unique that they are the only ones leading to metal complex-based conductors and superconductors is still unanswered and remains a contemporary research challenge. The shape, packing arrangement, and redox properties have usefully directed the investigation toward potential molecule candidates. Electronic structure determination is irreplaceable either for understanding some interesting transport properties of a given compound, as shown in the case of (SMeEt$_2$)[Pd(dmit)$_2$]$_2$, or for explaining the subtle differences in these properties due to slight changes in the geometry, as shown by the comparison in this work between (SMeEt$_2$)[Pd(dmit)$_2$]$_2$ and α-TTF[Pd(dmit)$_2$]$_2$ or previously between Cs[Pd(dmit)$_2$]$_2$ and δ-TTF[Pd(dmit)$_2$]$_2$.[65,71] However, really unfailing guide rules based on some clear-cut theory are still to be found. For example, it was generally admitted that the use of small countercations should enhance the interaction between the M(dmit)$_2$ units and, hence, the conductivity. The high conductivity of compounds with bulky cations such as PPN$^+$ and BTP $^+$ and the almost 2 orders of magnitude increase in the conductivity when going from (SMe$_3$)[Ni(dmit)$_2$]$_2$ to (SEt$_3$)[Ni(dmit)$_2$]$_z$ seem to be inconsistent with that prediction. On the other hand, the higher conductivity of the palladium compounds compared to the nickel compounds studied here seems to confirm a general trend previously observed for related systems.[14,15] For the time being, and in the absence of foolproof guidelines, further research in this field will result, as before, from serendipitous procedures, and progress will be based on trial-and-error procedures, involving the design, preparation, and evaluation of new systems by using empirical selection criteria.

Acknowledgment. This work was sponsored in part by an EEC Molecular Conductors Network Award (Grant No. ERB4050PL930085) and a grant from the Conseil Régional Midi-Pyrénées (CCRRDT Grant No 9300690). We thank D. de Montauzon for assistance in electrochemical studies. C.R. thanks the Departament d'Ensenyament de la Generalitat de Catalunya for a predoctoral fellowship. E.C. thanks the CNRS for granting a sabbatical leave that made the stay at ICMAB possible.

Supporting Information Available: Figures showing cyclic voltammograms of (PPN)[Ni(dmit)$_2$], (BTP)[Ni(dmit)$_2$], (SMe$_3$)$_2$[Pd(dmit)$_2$], (NEt$_4$)[Pd(dddt)$_2$], and (NBu$_4$)[Pt(dtdt)$_2$], single-crystal conductivity of (PPN)[M(dmit)$_2$]$_z$ and (BTP)[M(dmit)$_2$]$_z$ (M = Ni, Pd), and single-crystal conductivity of (SMe$_y$Et$_{3-y}$)[Ni(dmit)$_2$]$_z$ (y = 0, 1, 3) (Figures S1, S2, and S3). Elemental analyses and IR data for starting (cation)$_n$[ML$_2$] complexes (L = dddt^{2-}, dtdt^{2-}, dmit^{2-}; n = 0, 1, 2; M = Ni, Pd, Pt) (Table S1), electrocrystallization conditions, conductivity values, and elemental analyses for [M(dddt)$_2$][M′(dmit)$_2$]$_x$ and (cation)[M(dmit)$_2$]$_z$ compounds with cation = PPN$^+$, BTP$^+$ (Tables S2 and S3), electrocrystallization conditions and conductivity values for (SMe$_y$Et$_{3-y}$)[M(dmit)$_2$]$_z$ compounds (Table S4), additional relevant parameters of data collections and refinements (Table S5), hydrogen atomic parameters (Tables S6−S11, anisotropic thermal parameters (Tables S12−S18), and bond distances and angles (Tables S19−S25) for compounds **1**−**7**, and cyclic voltammetry data (Tables S26 and S27). (29 pages). Ordering information is given on any current masthead page.

IC9600341